Mehmet Fazıl Kapçı

A Master's Thesis

AGU 2021

INVESTIGATION OF HYDROGEN EMBRITTLEMENT BY A MULTI-SCALE MODELLING APPROACH

A THESIS
SUBMITTED TO THE DEPARTMENT OF ADVANCED MATERIALS AND NANOTECHNOLOGY
AND THE GRADUATE SCHOOL OF ENGINEERING AND SCIENCE
OF ABDULLAH GUL UNIVERSITY
IN PARTIAL FULFILLMENT OF THE REQUIREMENTS
FOR THE DEGREE OF
MASTER OF SCIENCE

By
Mehmet Fazıl KAPÇI
August 2021

INVESTIGATION OF HYDROGEN EMBRITTLEMENT BY A MULTI-SCALE MODELLING APPROACH

A THESIS
SUBMITTED TO THE DEPARTMENT OF ADVANCED MATERIALS AND NANOTECHNOLOGY
AND THE GRADUATE SCHOOL OF ENGINEERING AND SCIENCE OF ABDULLAH GUL UNIVERSITY
IN PARTIAL FULFILLMENT OF THE REQUIREMENTS
FOR THE DEGREE OF
MASTER OF SCIENCE

By
Mehmet Fazıl KAPÇI
August 2021

SCIENTIFIC ETHICS COMPLIANCE

I hereby declare that all information in this document has been obtained in accordance with academic rules and ethical conduct. I also declare that, as required by these rules and conduct, I have fully cited and referenced all materials and results that are not original to this work.

Name-Surname: Mehmet Fazıl KAPÇI

Signature :

REGULATORY COMPLIANCE

M.Sc. thesis titled "Investigation of Hydrogen Embrittlement by a Multi-scale Modelling Approach" has been prepared in accordance with the Thesis Writing Guidelines of the Abdullah Gül University, Graduate School of Engineering & Science.

Prepared By	Advisor
Mehmet Fazıl KAPÇI	Burak BAL
Signature	Signature

Head of the Advanced Materials and Nanotechnology Program

Assist. Prof. Fahri ALKAN

Signature

ACCEPTANCE AND APPROVAL

M.Sc. thesis titled "Investigation of Hydrogen Embrittlement by a Multi-scale Modelling Approach" and prepared by Mehmet Fazıl KAPÇI has been accepted by the jury in the Advanced Materials and Nanotechnology Graduate Program at Abdullah Gül University, Graduate School of Engineering & Science.

05 /08 / 2021

(Thesis Defense Exam Date)

JURY:

Advisor: Doç. Dr. Burak BAL .....

Member: Dr. Öğr. Üyesi Çağatay YILMAZ .....

Member: Dr. Öğr. Üyesi Murat AYDIN .....

APPROVAL:

The acceptance of this M.Sc. thesis has been approved by the decision of the Abdullah Gül University, Graduate School of Engineering & Science, Executive Board dated ….. /….. / …….. and numbered ……..……. .

…….. /…….. / ……..

(Date)

Graduate School Dean
Prof. Dr. Hakan USTA

ABSTRACT

INVESTIGATION OF HYDROGEN EMBRITTLEMENT BY A MULTI-SCALE MODELLING APPROACH

Mehmet Fazıl KAPÇI

MSc. in Advanced Materials and Nanotechnology

Advisor: Assoc. Prof. Dr. Burak BAL

August 2021

Hydrogen exposure of metallic materials during their service times or during the application of processes e.g. machining, welding, electroplating leads to degradation of the mechanical properties which is a phenomenon known as hydrogen embrittlement. Diffused hydrogen into metal can accumulate in crystal defects and alter the mechanical behavior under loading. In this thesis, diffusion of the hydrogen as well as the atomistic mechanisms of dislocation mobility depending on the presence of hydrogen were investigated for two edge dislocation systems that are active in the plasticity of α-Fe, specifically ½<111>{110} and ½<111>{112}. In particular, the glide of the dislocation pile-ups through a single crystal, as well as transmission of the pile-ups across the grain boundary were evaluated in bcc iron crystals that contain hydrogen concentrations in different amounts. Additionally, the uniaxial tensile response under a constant strain rate was analyzed for the aforementioned structures. Lastly, diffusion and back-diffusion of the hydrogen into bcc, fcc, and hcp crystal structures were investigated with numerical models. The results reveal that the presence of hydrogen decreases the velocity of the dislocations – in contrast to the commonly invoked HELP (Hydrogen-enhanced localized plasticity) mechanism -, although some localization was observed near the grain boundary where dislocations were pinned by elastic stress fields. In the presence of pre-exisiting dislocations, hydrogen-induced hardening was observed as a consequence of the restriction of the dislocation mobility under uniaxial tension. Furthermore, it was observed that hydrogen accumulation in the grain boundary suppresses the formation of new grains that leads to a hardening response in the stress-strain behaviour which can initiate brittle fracture points.

Keywords: Hydrogen Embrittlement, Molecular Dynamics, Dislocation, Fracture

ÖZET

HIDROJEN GEVREKLİĞİNİN ÇOK ÖLÇEKLİ MODELLEME YAKLAŞIMIYLA İNCELENMESİ

Mehmet Fazıl KAPÇI
İleri Malzemeler ve Nanoteknoloji Anabilim Dalı Yüksek Lisans
Tez Yöneticisi: Doç. Dr. Burak BAL
Ağustos 2021

Malzemelerin kullanım sırasında veya talaşlı imalat, kaynak, elektro kaplama gibi işlemler sırasında hidrojene maruz kalması mekanik davranışlarının bozulmasına sebebiyet verebilmektedir. Hidrojen gevrekliği olarak bilinen bu durumda atomik hidrojen metal kristali içerisine nüfuz ederek buradaki kristal kusurlar etrafında birikmekte ve bu yapıların yük altındaki davranışlarını değiştirmektedir. Bu tez çalışmasında hidrojen difüzyonu ve bunun yanında hidrojen etkisinde dislokasyon hareketliliğinin atomik mekanizmaları, α-Fe'nin plastisite davranışında aktif olan iki kayma sistemi, spesifik olarak ½<111>{110} ve ½<111>{112} kenar dislokasyonları için incelenmiştir. Detaylı olarak farklı hidrojen yoğunluklarında tek kristal içinde dislokasyon yığını kaymaları, bunun yanında tane sınırı içeren yapılarda dislokasyonun tane sınırından geçişi bcc demir kristallerinde değerlendirilmiştir. Bununla beraber, bahsi geçen yapıların sabit gerilme oranı altında tek yönlü çekme davranışının analizleri yapılmıştır. Son olarak bcc fcc ve hcp kristal yapılarda hidrojen difüzyon ve geri difüzyonu nümerik modeller ile incelenmiştir. Elde edilen sonuçlara göre sıkça kullanılan HELP mekanizmasının aksine hidrojenin dislokasyon hızını azalttığı görülmüştür. Buna karşın tane sınırı elastik gerilmelerinin etkisiyle bu bölgelerde hidrojen ile dislokasyon lokalizasyonu da gözlenmiştir. Hidrojenin önceden varolan dislokasyonların hızını düşürmesi ile tek yönlü çekme davranışında sertleşme görülmüştür. Ayrıca, hidrojenin tane sınırlarında birikimi yeni tane sınırı oluşumlarını baskılamakta ve gevrek kırılmalara sebebiyet verebilen sertleşme davranışını arttırmaktadır.

Anahtar kelimeler: Hidrojen Gevrekliği, Moleküler Dinamik, Dislokasyon, Kırılma

Acknowledgements

I would like to express my sincere gratitude to my advisor, Assistant Professor Burak BAL for his enormous support and guidance in all my research that started from my B.Sc. degree and has continued until now. Also, I would like to give special thanks to Professor Christian SCHÖN and Assistant Professor Fahri ALKAN for their valuable advices during my studies.

I also thank M^2EGACM research group members for their collaborations during my research. Additionally, I would like to thank my friends Fatih EROĞLU, Enes Sedat ÇAĞLAR and Beytullah EFEYİK for their supports.

Finally, I would like to express my deep gratitude to my family for their continues supports and understandings.

TABLE OF CONTENTS

LIST OF FIGURES

LIST OF TABLES

LIST OF ABBREVIATIONS

BCC	Body Centered Cubic
DXA	Dislocation Extraction Algorithm
EAM	Embedded Atom Method
FCC	Face Centered Cubic
HCP	Hexagonal Close Packed
HE	Hydrogen Embrittlement
HEDE	Hydrogen Enhanced Decohesion
HELP	Hydrogen Enhanced Localized Plasticity
HVEM	High-Voltage Electron Microscope
LAAMPS	Large-Scale Atomic Molecular Massively Parallel Simulator
MD	Molecular Dynamics
NPT	Isothermal-Isobaric
NVE	Microcanonical
SEM	Scanning Electron Microscopy
TDS	Thermal Desorption Spectroscopy
TEM	Transmission Electron Microscope

To My Family

Chapter 1

1. Introduction

In the first chapter of this thesis titled “Investigation of Hydrogen Embrittlement by a Multi-Scale Modelling Approach”, the hydrogen embrittlement phenomenon is introduced. First, the effects of hydrogen that lead to degradation of mechanical properties of metallic materials are discussed in detail with several proposed mechanisms in literature. Moreover, modelling methods of the hydrogen concentration in the crystal defect sites at different length and time scales are represented by focusing on the edge dislocation and symmetric tilt grain boundary where the effects of hydrogen on the behaviors of these defects are included in the upcoming chapter (Chapter 2). Finally, the aim and the objectives of the thesis were explained in the second subsection.

1.1 Motivation and Background

1.1.1 Hydrogen Embrittlement

Hydrogen embrittlement (HE) is a type of fracture mechanism of metallic materials that can affect a wide range of applications by leading to failure of materials during their service times [1]. In particular, materials show a premature fracture or they lose their toughness unexpectedly due to the atomic hydrogen diffused into crystal lattice. Especially the high strength steels, aluminum, titanium, and nickel alloys possess a high susceptibility to hydrogen embrittlement which are used as structural components in the automotive and aerospace industries [2]. Additionally, detrimental effects of hydrogen can be seen in the application areas that contain high hydrogen contaminant in the environment such as oil/gas or nuclear industries. Beside all these, during the production, cathodic protection, welding, or electroplating processes, metals can expose to high amount of hydrogen that can lead to reduction in mechanical strength and elongation [3–5]. Additionally, using the hydrogen as an alternative energy source also brings up the problem of hydrogen related failures. Increasing demand on

the new alternative energy sources is gaining importance gradually due to the consequences of the harmful effects and shortage of the fossil fuels. Although the hydrogen energy stands as a possible solution for this issue, degradation effect of the hydrogen on metallic materials during the production, storage, and transportation of the hydrogen is one of the key challenge to use this alternative energy in a wide range of applications [6].

Degradation effect of atomic hydrogen when it diffuses into metallic materials is known for over a century and many investigations have been conducted to understand the underlying mechanisms of this effect. After the diffusion of the hydrogen into material, it can be accumulated in several defect sites, e.g. surface/subsurface, the cores of the edge and screw dislocations, grain boundaries, and vacancies. Figure 1.1 illustrates the possible accumulation sites of the hydrogen after diffusion into microstructure [7].

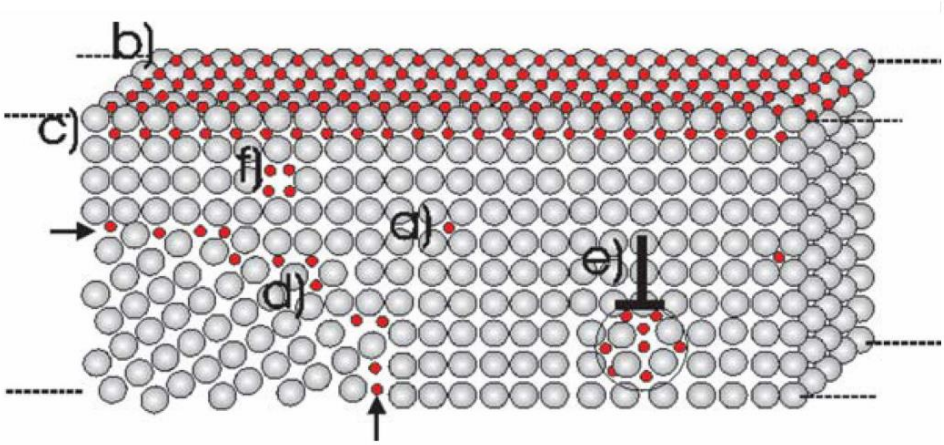

Figure 1.1 Possible hydrogen accumulation sites in the microstructure. Hydrogen a) in interstitial positions in the lattice, b,c) trapped hydrogen in surface and subsurface, d) in grain boundary, e) in dislocation core, f)in vacancy (adopted from [7]).

Once hydrogen atom diffuses into these crystal defects, depending on the concentration, it can alter the volume, potential energy, and stress field of the defect by changing the orientations of the atoms around [8–10]. Eventually, the behaviors of these defects as well as the interactions with other defects are influenced by the presence of the hydrogen atoms. Thus, understanding the hydrogen-defect interactions constitute a significant place in order to evaluate and prevent HE phenomenon. Although the underlying mechanisms of HE have been investigated by many studies until now, there are 3 main commonly invoked mechanisms in the literature. These mechanisms can be

listed as HEDE (hydrogen enhanced decohesion), HELP (hydrogen enhanced localized plasticity), and hydrogen induced hydride formation and fracture mechanisms [11]. Illustrations of the mechanisms are given in the Figure 1.2.

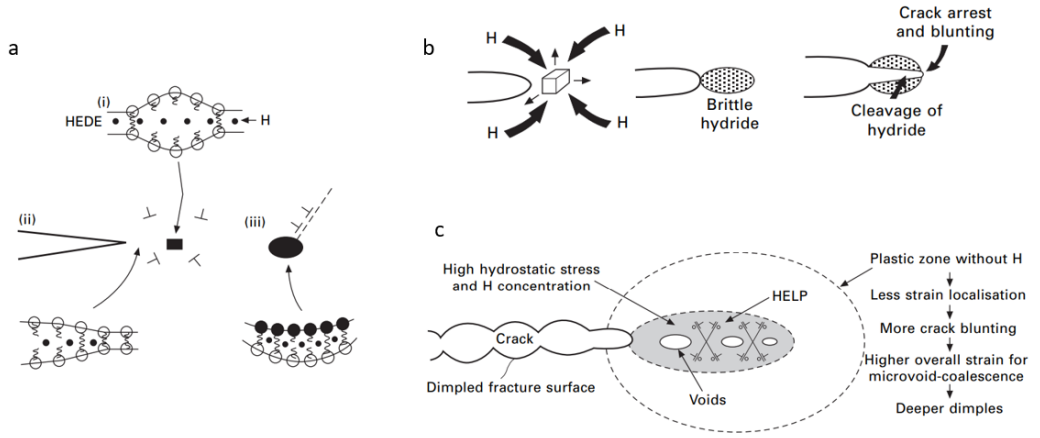

Figure 1.2 Hydrogen embrittlement mechanisms. a) Hydrogen enhanced decohesion (HEDE) (adopted from [11]), b) hydrogen induced hydride formation (adopted from [11]), c) Hydrogen enhanced localized plasticity (HELP) (adopted from [11]).

In the HEDE mechanism, it was proposed that atomic hydrogen decrease the cohesive energy between the lattice layers which leads to separation of these layers as a consequence of weakened interatomic bonds between metal atoms[12]. Additionally, it was stated that when the hydrostatic stress is high in a region e.g. ahead of the crack tip or the regions near the other defects such as inclusions and dislocations, hydrogen is keen to accumulate in these regions due to elastic stresses and dilation of the volume between the surrounding atoms. Thus, accumulation of atomic hydrogen in these sites can lead to separation of the atomic layers under lower stresses [13,14]. For the materials that contains hydride forming elements such as V, Zr, Nb, Ta, Ti etc., another mechanism, stating that hydrogen induced hydride formation is responsible for premature fracture, was proposed. Increase in the hydrogen content depending on hydrostatic stress, induces the formation of brittle hydrides which eventually starts the cleavage along the brittle hydride phase [15–17]. The third mechanism is HELP (hydrogen enhanced localized plasticity). It was stated in this mechanism that presence of the hydrogen in the lattice, increases the mobility of dislocations and has a shielding effect for the dislocation-dislocation and dislocation other defects interactions.

Eventually, reduction in the elastic stresses between defects leads to localized plastic region in the microstructure and facilitates the propagation of the cracks [18,19].

Hydrogen induced fracture was investigated by many experimental studies with different material microstructures, loading conditions and hydrogen content [20–24]. After charging the samples with hydrogen, various types of loadings can be applied to the materials e.g. tensile, impact, fatigue loading to determine the effect of hydrogen on macroscopic mechanical response. Additionally, the fracture surface evaluations can be conducted via different microscopy techniques such as optical microscopy, scanning electron microscopy (SEM) or transmission electron microscopy (TEM) to evaluate the type of fracture which could be intergranular fracture due to the hydrogen segregation in the grain boundaries or brittle transgranular fracture by facilitated crack propagation in the hydrogen presence. On the other hand, revealing the atomistic origin of the hydrogen embrittlement and H-defect interactions requires using of modelling methods in both atomistic scales and macro scales. Altered macroscopic behaviors of the materials after the hydrogen exposure are rooted in various factors take place in the short timescales including hydrogen-defect and also defect-defect interactions under the influence of hydrogen. Thus, modelling the atomistic scale behaviors and integration of the outputs of these models into the macroscale models is important for a comprehensive understanding of the HE phenomenon.

1.1.2 Modelling of Hydrogen Concentration in the Crystal Defects

Investigating the diffusion of the hydrogen into crystal defect and revealing the concentration in this defect sites relative to lattice is important to understand hydrogen embrittlement phenomenon. Several modelling techniques can be utilized in this context. In this part, modelling the hydrogen concentration was discussed for the edge dislocation and symmetric tilt grain boundary in accordance with the further studies presented in the thesis.

One way to observe the hydrogen diffusion and concentration in the vicinity of an edge dislocation is the steady-state model by using diffusion-convection equation and continuum level stress field of the dislocation. Considering a body with a volume V and surface S, mass conservation states that the rate of change in the hydrogen concentration in V is related to the flux through the surface S as

$$\frac{\partial}{\partial t}\int c dV + \int J\, n dS = 0 \qquad \textbf{(1.1)}$$

where $\frac{\partial}{\partial t}$ is the partial derivative with respect to time, c is the hydrogen concentration, J is flux and n is outward unit normal vector to ∂V. The flux is proportional to the chemical potential gradient, which is driving force for diffusion, diffusion coefficient and hydrogen concentration as follows [25]:

$$J = -m\nabla\mu = -\frac{Dc}{RT}\nabla\mu \quad \textbf{(1.2)}$$

where m is mobility, D is the diffusion coefficient, R is gas constant, T is temperature and μ is chemical potential. Negative sign indicates that the transport is from high to low chemical potential. From fundamental thermodynamic relations the chemical potential of the hydrogen atoms can be expressed as considering the Helmholtz free energy [26]:

$$\mu = \left(\frac{\partial\psi}{\partial c}\right)_{T,P} = \mu_0 + RTlnc + \mu_\sigma \quad \textbf{(1.3)}$$

where μ_0 is the reference chemical potential and μ_σ is stress dependent part of the chemical potential which can be calculated as

$$\mu_\sigma = -\frac{\sigma_{kk}}{3}V_H \quad \textbf{(1.4)}$$

where V_H is partial molar volume of hydrogen and σ_{kk} is applied stress. The elastic stress field of the edge dislocation in the x and y directions are defined as

$$\sigma_{xx} = -\frac{Gby\,(3x^2+y^2)}{2\pi\,(1-\vartheta)(x^2+y^2)^2}\,,\ \sigma_{yy} = -\frac{Gby(x^2-y^2)}{2\pi\,(1-\vartheta)(x^2+y^2)^2} \quad \textbf{(1.5)}$$

where G is the shear modulus, b is Burgers vector and, ϑ is Poisson's ratio. As an illustration, figure 1.3 represents the elastic stresses σ_{xx} and σ_{yy} around the edge dislocation in bcc iron crystal.

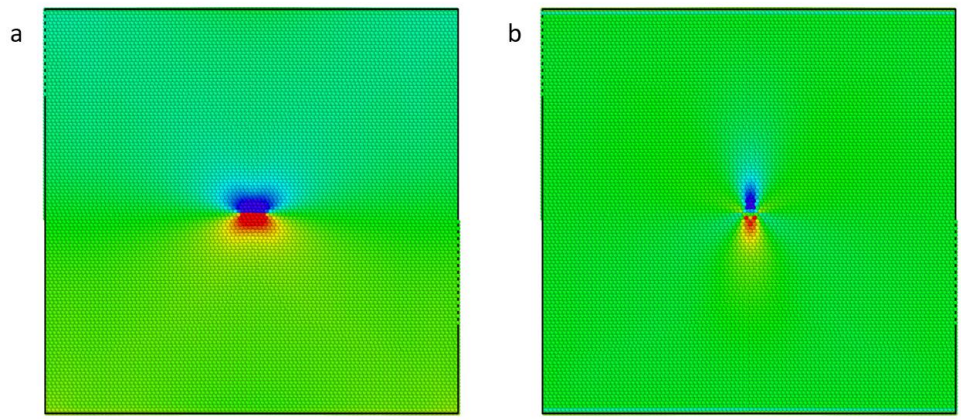

Figure 1.3 a) σ_{xx} and b) σ_{yy} stress field of the edge dislocation in the center. Blue colors represent compressive and red colors represents tensile region

Substitution of the Eq. (1.3) and (1.4) into Eq. (1.2) the flux can be obtained as

$$J = -D\nabla c - \frac{DV_H}{RT} c\nabla \frac{\sigma_{kk}}{3} \tag{1.6}$$

Considering the Fick's first law with the addition of convective term, flux can also be defined as

$$J = -D\nabla c - uc \tag{1.7}$$

where u is the velocity of the hydrogen transport around dislocation driven from the chemical potential gradient which can be obtained as

$$u = \frac{DV_H}{RT} \nabla \frac{\sigma_{kk}}{3} \tag{1.8}$$

Finally, the partial derivative of hydrogen concentration with respect to time can be related with flux as follows

$$\frac{\partial c}{\partial t} = -\nabla J = D\nabla^2 c - \frac{DV_H}{RT}\left(\frac{c\nabla^2 \sigma_{kk}}{3} + \nabla c \nabla \frac{\sigma_{kk}}{3}\right) \tag{1.9}$$

Utilizing this equation to the FE (Finite Element) method for the bcc iron by using the diffusion coefficient of hydrogen in the iron gives the 2D steady state hydrogen concentration around the dislocation (Figure 1.4). It can be observed from the figure that hydrogen tends to accumulate in the core of dislocation and in the tensile region whereas the compressive region has a lower hydrogen concentration.

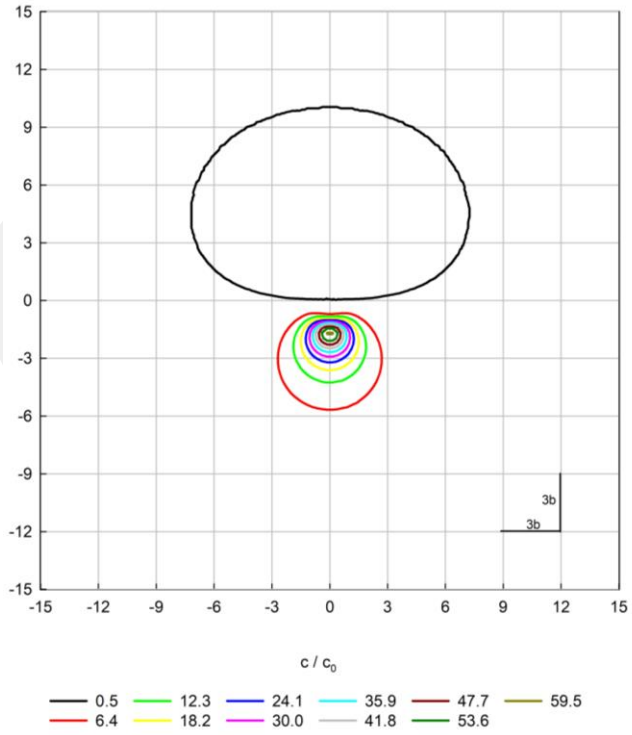

Figure 1.4 FEM analysis of hydrogen concentration around the edge dislocation (dislocation is located in the center x=0, y=0, initial hydrogen c_0=1).

Additionally, classical molecular dynamics (MD) method is another useful tool to evaluate the hydrogen concentration around the crystal defects. In order to model the hydrogen in the defects, an interatomic potential should be utilized to define the interaction between metal and hydrogen atoms where the parameters are obtained by ab-initio simulations. Currently, there are several interatomic potentials in the literature that define binary Fe-H interaction including EAM (embedded atom method), MEAM (modified embedded atom method), and Tersoff–Brenner potentials [27–30]. After the definition of the interatomic potential and generation of the simulation cell with defects, MD simulations can be performed including energy minimization and equilibration under pressure and temperature. Thus, hydrogen atoms can either accumulate in crystal defects or stay in the lattice in interstitial positions. Figure 1.5 demonstrates the hydrogen concentration in the bcc iron lattice and in the symmetric tilt grain boundary.

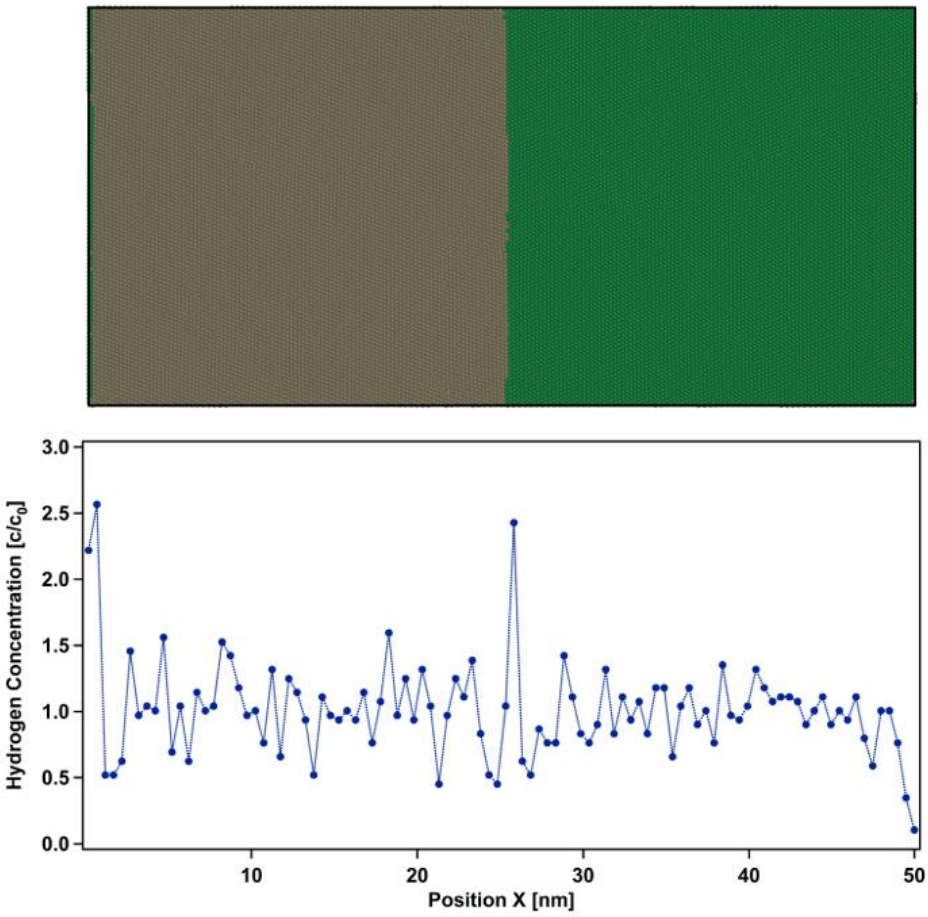

Figure 1.5 Hydrogen concentration obtained by MD method in grain boundaries and crystal lattice. Brown and green colors represents different grains and initial hydrogen concentration in the lattice $c_0 = 1$.

1.2 The Aim and Objectives

In this thesis, diffused hydrogen and crystal defect interactions are investigated in order to understand the atomistic mechanism of HE. Molecular Dynamics (MD) method was utilized for (body-centered cubic) bcc iron nanostructures that contains dislocation and grain boundaries. Specifically, the simulations were performed on 3 different structures; 2 single crystals that contain edge dislocations in different glide planes, and 1 bicrystal that also contains edge dislocations. For each of the three simulation set, hydrogen atoms were introduced in different concentrations. After that, each structure was exposed to shear and tensile loadings respectively. Thus, dislocation mobility as well dislocation-grain boundary interactions was evaluated under the influence of hydrogen. Additionally, effects of the altered responses of crystal defect on the overall mechanical behavior were observed by the tensile loading simulations. Finally, 1D and 2D transient diffusion of the hydrogen were modelled in the macroscale for the materials that possess bcc, fcc, and hcp crystal structures. Also, these simulations were performed in a timescale which is comparable with the charging times of the metallic specimens to use in the experimental studies.

Chapter 2

2. The Role of Hydrogen in the Edge Dislocation Mobility and Grain Boundary-Dislocation Interaction in α-Fe

2.1 Introduction

The embrittlement effect of hydrogen in metals was firstly discovered in 1875 by Johnson when studying changes of the macroscopic mechanical properties of a piece of iron that had been immersed in hydrochloric and sulphuric acids [31]. The presence of H in the metal facilitates the transition from ductile to cleavage type in the macroscopic fracture process when applying external stresses. This degradation of the mechanical properties causes failures of the material in a great number of engineering applications such as storage tanks, oil gas pipelines, structural components relying on high-strength steels and alloys, etc. [32–36]. Reduction in the yield and tensile stresses by the effect of hydrogen was observed in many previous studies including the deformation at slow, quasistatic, and high strain rates [37–40]. Additionally, hydrogen was reported to decrease ductility, facilitate crack propagation and, decrease fracture toughness that can result in brittle transgranular or intergranular crack formation in the microstructure [41–43]. Nonetheless, degradation of these properties by the presence of hydrogen depends upon several factors, such as hydrogen content exposure, mechanical state, and microstructural properties of the material [7,44]. There exist many models and theories which try to explain the embrittlement mechanism of metals due to hydrogen [11,45,46], and it is imperative to understand the underlying complexities involved. Discovering the fundamental mechanisms of hydrogen embrittlement (HE) requires information about the source of hydrogen - usually via chemical absorbtion of hydrogen atoms from the metal surface, or due to a release of hydrogen from chemical reactions inside the material -, and also about the diffusion of hydrogen through the lattice and its interaction with microstructural trap sites such as dislocations and grain boundaries [47,48].

Although the exact mechanism of hydrogen embrittlement remains unclear and various factors can contribute to the ultimate response, there are three generally accepted main mechanisms: hydrogen enhanced decohesion, hydride formation, and hydrogen enhanced localized plasticity. The hydrogen enhanced decohesion (HEDE) mechanism suggests that the diffused hydrogen decreases the cohesive energy between the metal atoms in the lattice and weakens the bonding across the atoms at the crack tip, which leads to the sequential separation of the layers and enhancement of the crack propagation under tensile stress [12,49]. Additionally, many experimental and theoretical studies support a mechanism according to which the accumulated hydrogen along grain boundaries can lead to an increased likelihood of fracture by intergranular crack formation [50–53]. Finally, the hydride formation mechanism suggests that regions with high hydrostatic stress, such as those ahead of the crack tip, can accumulate a large amount of hydrogen. This leads to the formation of brittle hydride phases, in particular, in the presence of hydride forming alloying elements V, Zr, Nb, Ta, Ti etc., which results in the propagation of the crack through the brittle phase [11,54]. For systems that do not form hydrides, hydrogen enhanced localized plasticity (HELP) is another frequently invoked mechanism involving the movement of dislocations: Based on the examination of fracture surfaces, Beachem [55] proposed the enhancement of the dislocation mobility in the presence of mobile hydrogen, which leads to an increased plasticity localized at the crack tips and thus causes brittle cleavage already for low applied stresses. Subsequently, this theory was supported by theoretical studies of Birnbaum and Sofronis [56]. Beside noting the effect of hydrogen on the velocity of the dislocations, they also claimed that hydrogen can shield the elastic stresses facing the dislocation due to elastic obstacles such as other dislocations, thereby contributing to the enhanced localized plasticity.

Dislocation behavior in materials containing hydrogen has also been investigated by in-situ TEM and HVEM tools [57,58]. It was proposed that the presence of hydrogen increases the dislocation velocities, and that stress shielding can reduce the distances among dislocations, resulting in pile ups, and between dislocations and defects that can serve as pinning points of the dislocations such as grain boundaries and solutes. Again, it has been observed that in the presence of hydrogen, the cracks can propagate already under low stresses, due to the localized plastic behavior ahead of the crack tip which is associated with an enhanced dislocation velocity and higher emission rate of new dislocations from the crack tip. However, due to the small size of the hydrogen

atoms and the difficulty to keep track of the dislocations in-situ, it is difficult to establish an explicit and statistically valid correlation between the dislocation mobility and the hydrogen concentration only from experimental data. Therefore, atomistic modelling of the hydrogen-defect containing structures is required to elucidate the underlying mechanisms.

There exist many studies investigating the role of hydrogen on the embrittlement mechanism via molecular dynamics simulations. Several investigations of the crack propagation in α-iron and nickel crystals reveal that hydrogen accumulated around the crack tip can inhibit the dislocation emission that leads to a ductile to brittle failure transition ahead of the crack tip [59–63]. Furthermore, hydrogen segregation along the grain boundaries and intergranular cleavage leading to a decrease of the cohesive energy has also been observed for various grain boundary orientations and grain sizes [64,65].

An important phenomenon to be understood is the role of hydrogen in the dislocation mobility and in the effective interaction of the dislocation with other defects. Several atomistic studies support the claim that hydrogen enhances the dislocation mobility and leads to a shielding of the stresses acting on dislocations [62,66]. On the other hand, in a study of the effect of hydrogen on α-iron ½<111>{110} edge dislocation pile ups, Song and Curtin [67] suggested that, unlike the previous TEM observations that supported the HELP mechanism, hydrogen does not increase the velocity of the dislocation but rather acts as a drag on the dislocations and thus decreases the velocity, and, in addition, no remarkable shielding can be observed when the dislocations encounter an elastic obstacle. Moreover, for the same dislocation orientation, Zhu et. al [68] claimed that vacancies containing hydrogen have a pinning effect on the dislocation, and that the strength of the pinning increases with the concentration of hydrogen trapped in the vacancy. Katzarov et. al [69] investigated the mobility of screw dislocations in α-iron using the kinetic Monte Carlo approach; they suggested that although for low hydrogen concentrations and applied stresses the velocity of dislocations increases, for higher hydrogen concentrations the dislocation velocity is lower than the one without hydrogen due to a dragging effect of the hydrogen atoms.

In the current study, the effect of hydrogen on the mobility of dislocations was investigated for two slip systems (½<111>{110} and ½<111>{112} edge dislocations) of $\boldsymbol{\alpha}$-iron by using molecular dynamics. Furthermore, the interaction of the ½<111>{112} dislocations with the Σ3<110>(112) symmetric tilt grain boundary was studied for

different hydrogen concentrations. Lastly, single crystal and bicrystal structures with dislocations exposed to tensile loadings were studied with the goal to understand the effect of hydrogen on the reaction of the system to applied tensile stresses.

2.2 Simulation Models

Molecular dynamics (MD) simulations were performed using LAMMPS (Large-scale Atomic/Molecular Massively Parallel Simulator) [70]on α-Fe crystals. Under pure shear loading, the mobility of ½<111>{110} and ½<111>{112} edge dislocations was examined for different hydrogen concentrations. The two orientations were chosen, because the <111> direction and the {110} and {112} planes are the most dominant slip systems in α-Fe, and in other bcc crystals as well [71,72]. Additionally, transmission across of the ½<111>{112} dislocations through the grain boundary in the presence of hydrogen was investigated by using a symmetric tilt-high angle grain boundary Σ3<110>(112) that has the lowest energy among the various grain boundary types of interest in this system [73]. Finally, uniaxial tensile loadings were performed for the three aforementioned configurations, in order to understand the effect of the hydrogen-defect interaction on the overall mechanical response.

The interatomic interactions among Fe and H atoms were described by using an EAM (embedded atom method) potential [27] where the total energy is given by [74]

$$E = \sum_i F_i(\rho_i(\vec{r}_i)) + \frac{1}{2}\sum_{j,i} \emptyset(r_{ij}) \quad \textbf{(2.1)}$$

F_i is the embedding energy as a function of ρ_i which denotes the electron density at position $\vec{r}_i$ and $\emptyset$ is the electrostatic pair potential between atoms i and j that only depends on their separation distance r_{ij}. Configurations were displayed by OVITO software [75], and dislocation analyses were performed using the dislocation extraction algorithm DXA [76]. Atomic stress calculations were conducted via the virial stress theorem [77];

$$\sigma_i = \frac{1}{V}\left(-m_i \frac{d\boldsymbol{u_i}}{dt} \otimes \frac{d\boldsymbol{u_i}}{dt} + \frac{1}{2}\sum_{j(\neq i)} \boldsymbol{r}_{ij} \otimes \boldsymbol{f}_{ij}\right) \quad \textbf{(2.2)}$$

where V is the volume that was calculated by the Voronoi tessellation method, m_i and u_i are the mass of the particle i and the displacement relative to a reference position, respectively, $\boldsymbol{r}_{ij}$ is the vector between particles i and j, and $\boldsymbol{f}_{ij}$ denotes the interatomic force between the two particles.

2.2.1 Dislocation Velocity in a Single Crystal

Single crystal simulations were conducted by using two different bcc iron crystallographic orientation sets of simulation cells with dimensions of 500 Å × 250 Å × 30 Å for the x, y and z directions, respectively. Each simulation cell contains five periodically arranged and equally spaced dislocations that were located 100 Å apart along a line in the x direction in the center of the cell; the glide planes are oriented along y and the Burger's vectors were oriented along the x direction (see Figure 2.1). Periodic boundary conditions were used along the x and z directions, and a shrink-wrapped boundary along the y direction was utilized for each simulation cell, i.e., atoms are encompassed by the boundary along the y direction. In order to observe the dislocation velocity under shear stress, a 25 Å region at the bottom ($y = y_{bottom}$) was kept fixed and a 25 Å region at the upper part ($y = y_{top}$) was treated as rigid; in this top region, every atom was exposed to a force parallel to the x direction, such that an average shear stress τ_{xy} of 1 GPa was established. Figure 2.1 illustrates the initial configuration used for the first set of simulations.

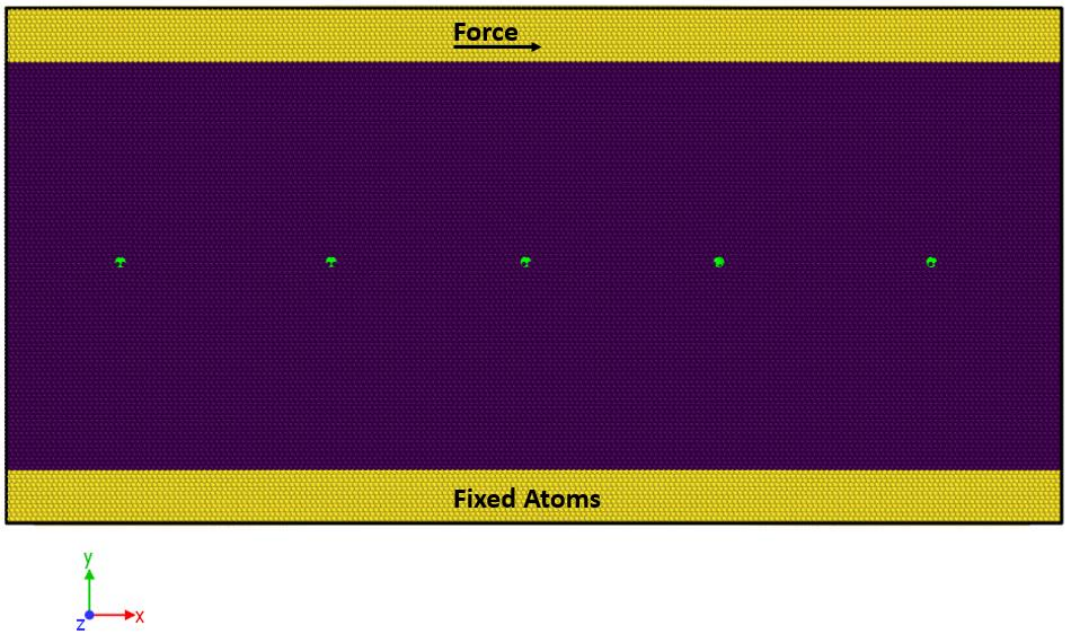

Figure 2.1 Initial configuration for the dislocation velocity simulations in a single crystal with ½<111>{110} dislocations [78].

For the first set, the directions [111], [1-10] and, [-1-12] of α-Fe were aligned along the x, y and z directions, respectively, with five equally spaced (periodic) ½<111>{110} dislocations along the center line parallel to the x direction. For the

second set, the [111], [-1-12] and [1-10] directions were oriented along x, y and z directions, respectively, with again five equally spaced ½<111>{112} dislocations along the center line in the x direction with the same simulation cell dimensions and initial boundary conditions. After constructing the initial configurations, hydrogen was introduced to each of the two orientation sets with concentrations of 0.25% H/Fe, 0.5% H/Fe and, 1% H/Fe. Figure 2.2 shows the configuration with 0.25% H/Fe concentration for the first set of orientations.

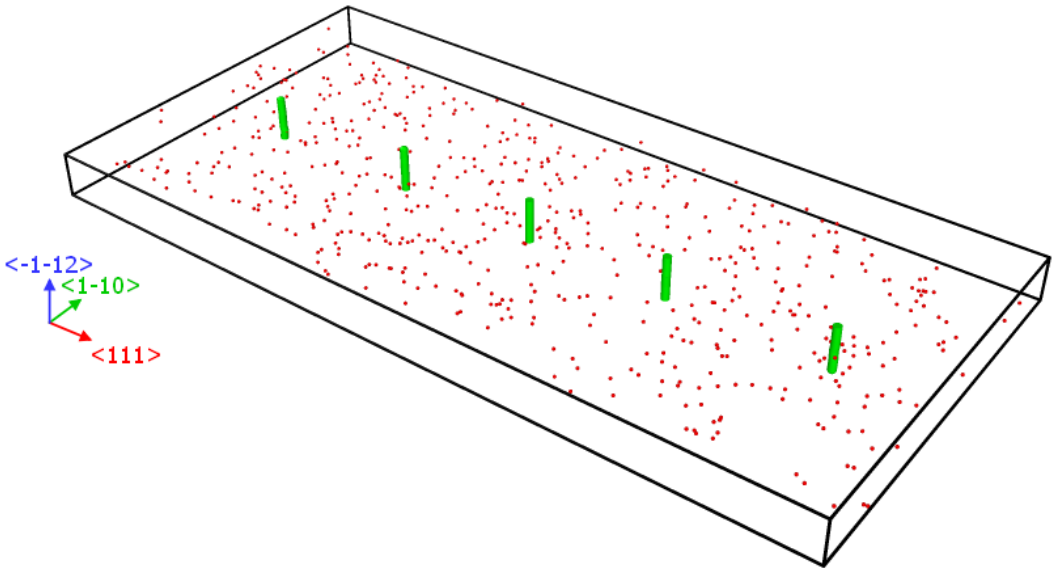

Figure 2.2 Initial configuration of the simulation cell containing five ½<111>{110} dislocations, with 0.25% H/Fe concentration. Recall: the directions [111], [1-10] and, [-1-12] of α-Fe are aligned along the x, y and z directions, respectively [78].

Prior to loading, the energy was minimized for each simulation cell and the system temperature was equilibrated via NVE ensemble simulations for 50 ps by rescaling the temperature of the atoms to 300 K in each step, in order to let the hydrogen atoms diffuse through the system; usually, the H-atoms reside at various interstitial positions in equilibrium. Finally, a constant average force was exerted on the atoms belonging to the upper part of the simulation cells (at $y = y_{top}$) parallel to the x direction, $\vec{F} = F_{avg}\hat{x}$, that is computed via the formula

$$F_{avg} = \frac{\tau_{xy} \times (l_x \times l_z)}{n} \quad \textbf{(2.3)}$$

Here, τ_{xy} is the shear stress exerted on the region that contains the dislocations, l_x and l_z are the length of the supercell along the x and z directions, and n is the total number of atoms in the rigid part at $y = y_{top}$. The loading stage simulation was

performed for 50 ps for two crystallographic orientations and all hydrogen concentrations studied.

2.2.2 Grain Boundary-Dislocation Interaction

In order to evaluate the effect of hydrogen on the transition of the ½<111>{112} dislocations through the Σ3<110>(112) symmetric tilt grain boundary, a simulation cell of the same size as the one in the single crystal case was generated. The structure consisted of 2 crystals of equal size that were connected via a tilt grain boundary, and which contained a total number of 6 equally spaced dislocations. The normal vectors of the two grain boundary planes were oriented in the x direction, and the grain boundaries were located in the middle and at the border of the periodically repeated simulation cell. The initial configuration is shown in Figure 2.3. Regarding the hydrogen concentrations, we employed the same ones as we had for the single crystal simulations (0.25%, 0.5 % and 1%), and, similarly, the energy minimization step was followed by a NVE ensemble simulation at 300 K to equilibrate the temperature prior to shear loadings for 50 ps. For the shear loading, the force was again applied to the atoms at the upper part of the cell ($y = y_{top}$); however, a shear stress of 1.5 GPa was applied and the loading stage simulations were performed for 150 ps.

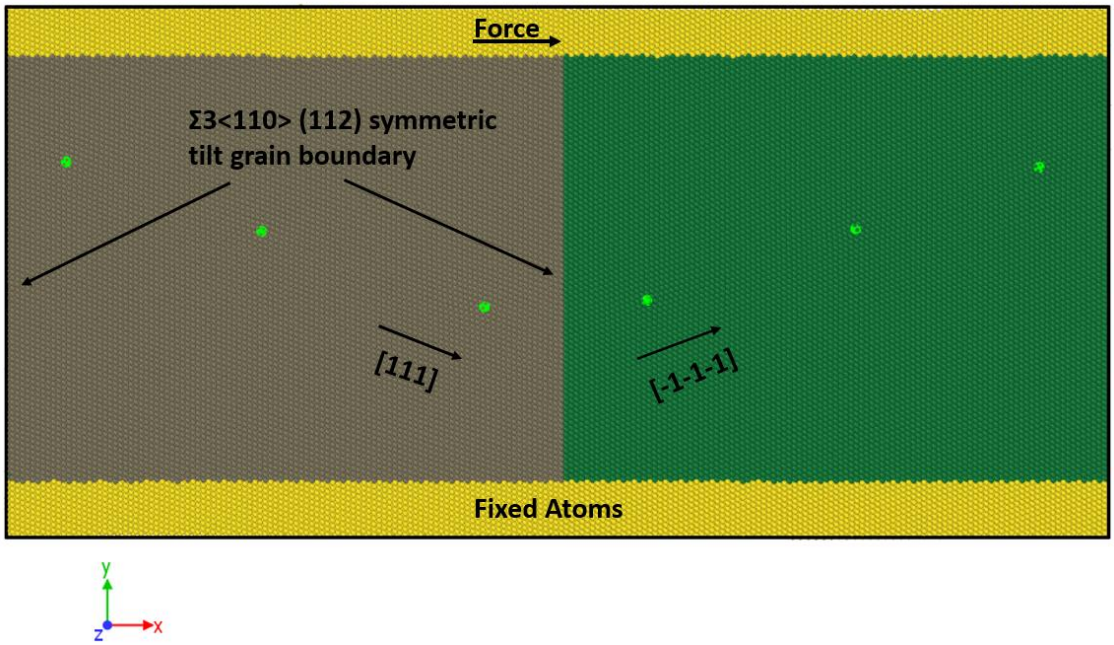

Figure 2.3 Initial configuration for the simulations containing six dislocations and two grain boundaries, one in the center and one at the border of the simulation cell [78].

2.2.3 Tensile Properties

Simulations of tensile properties were performed for each of the three systems in order to elucidate the mechanical response of the structures containing defects as function of hydrogen content. For the single crystals, not only the aligned sequence of five dislocations (figure 2.1) was used, but also the dislocations that had been randomly distributed through the simulation cell (figure 2.4), and for the bicrystal the same initial configuration (figure 2.3) was used. We first relaxed the hydrogen-free initial configurations at 0 GPa pressure, and afterwards equilibrated the temperature (in the NVE ensemble) and then the pressure (in the NPT ensemble) at 300 K and 0 GPa pressure for 50 ps with periodic boundary conditions in all three directions. We also employed periodic boundary conditions along the y direction rather than shrink-wrapping as in the previous simulations; since there are extra half planes of atoms for each dislocation at the upper side of the dislocations, new dislocations were formed and more dislocations were obtained for each simulation set. After this stage, hydrogen atoms were inserted into each structure, again with concentrations of 0.25%, 0.5% and 1%, and the temperature was equilibrated at 300 K. For all subsequent simulations, a uniaxial tensile load was applied parallel to the x direction with the strain rate of 10^{-3} 1/ps (10^{9} 1/s) with periodic boundaries in all directions up to a 50% strain. The simulations were then performed in the NPT ensemble by keeping the pressure at 0 GPa along y and z.

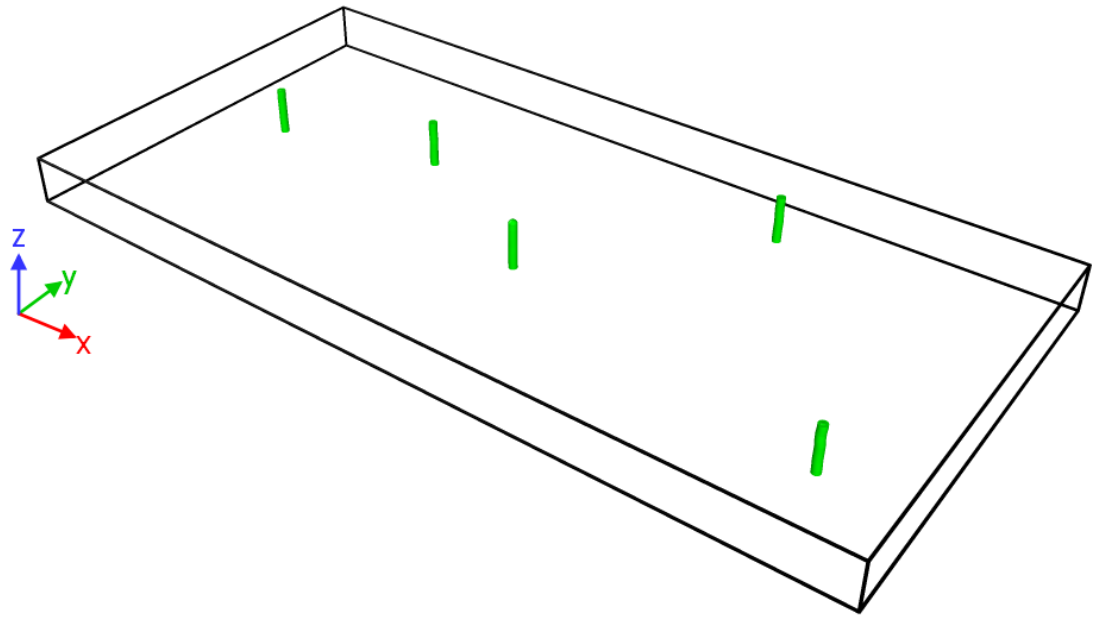

Figure 2.4 Randomly distributed five dislocations through the simulation cell for tensile simulations [78].

2.3 Results

2.3.1 Dislocation Velocity in a Single Crystal

Before evaluating the dislocation mobility under shear load, virial stresses and total energy of the dislocations were investigated after the temperature equilibration. The (local) total energies per atom of the Fe atoms within the 5 Å cut-off around the dislocation cores ($E_{dislocation}$) were calculated for each simulation cell (Figure 2.5a). Figure 2.5b shows the average normalized energy $\tilde{E}$ of the dislocations with respect to the energy of the reference crystal ($E_{reference}$) :

$$\tilde{E} = \frac{E_{dislocation} - E_{reference}}{|E_{reference}|} \quad . \tag{2.4}$$

For both systems, the local energy of the system with dislocations was larger than the one for the reference system if no hydrogen atoms had been added, i.e., $\tilde{E} > 0$, where the ½<111>{112} dislocations caused a larger energy increase than the ½<111>{110} dislocations. In both systems, it was found that the local energy of the crystal distortion at the dislocation cores was reduced by the hydrogen accumulation for each glide plane, where a larger energy change was observed for the ½<111>{112} dislocations. However, for a hydrogen concentration of 1%, both systems were found to be more stable when compared to the reference state, i.e., $\tilde{E} < 0$.

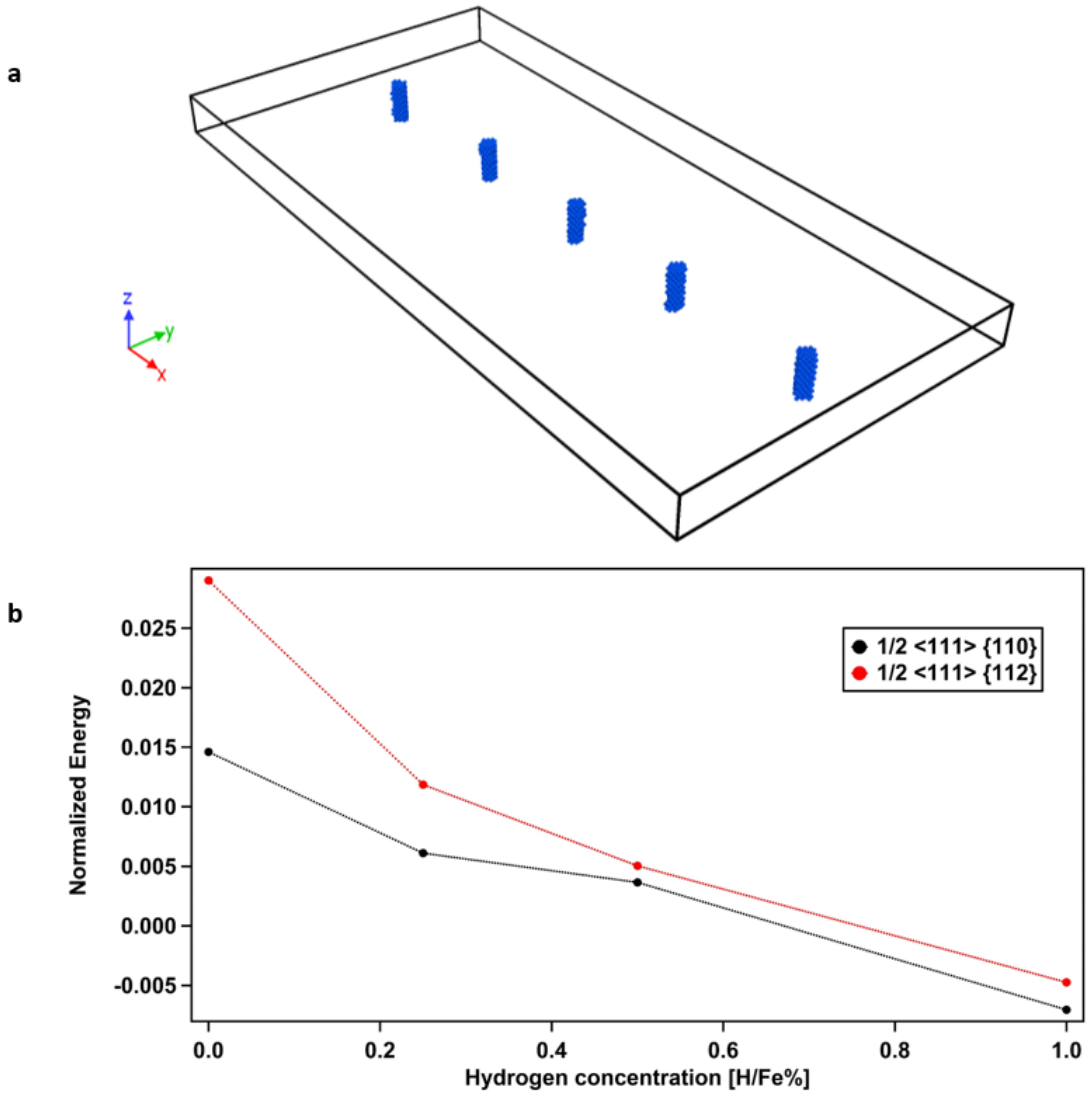

Figure 2.5 a) Fe atoms within the 5 Å cut-off from the dislocation cores in the case with ½<111>{112} dislocations and 0% hydrogen concentration. b) Normalized energy values for two glide planes and four hydrogen concentrations [78].

Furthermore, virial stresses in the x direction were evaluated both for the compressive and tensile region within a 40 Å wide (in the y-direction) band along the x direction above and below the line at y = 125 Å, on which the dislocations had been placed (Figure 2.6a). It was observed that hydrogen accumulation increases the compressive stress σ_{xx} in the 20 Å wide region above the dislocation core (125 Å < y < 145 Å) in the overall behavior; here, the 0.25% H concentration shows a larger stress value compared with the 0.5% case, for the ½<111>{112} dislocations (Figure 2.6b). A more monotonic increase in the magnitude of the stress field was observed in the tensile region, 105 Å < y < 125 Å, for both types of dislocations (Figure 2.6c), where hydrogen accumulation in the dislocation core reduced the stresses for both glide planes. It should

be noted that unlike the potential energy of alpha-Fe, the magnitude of the change in the stress was higher for the ½<111>{110} dislocations.

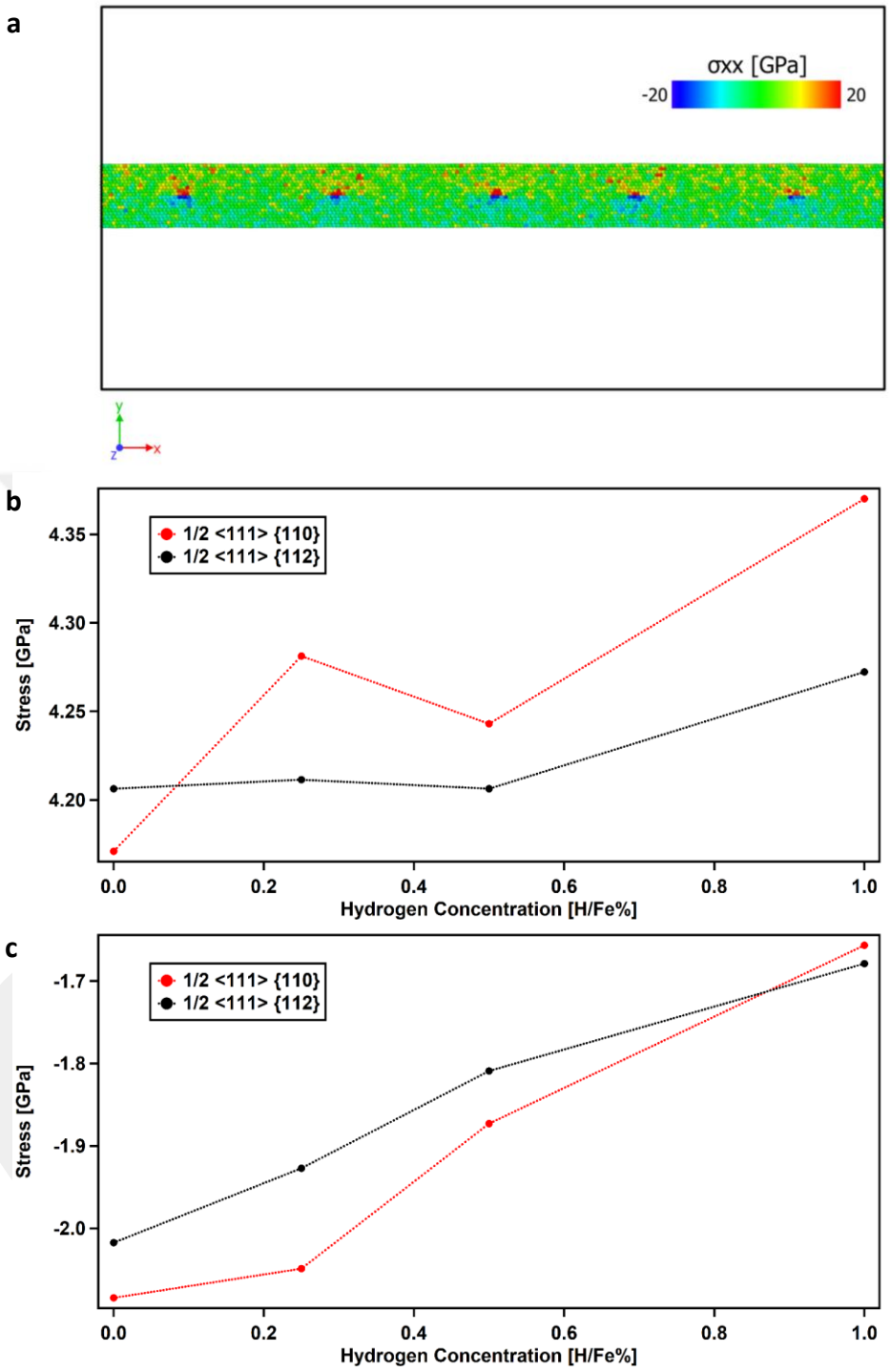

Figure 2.6 a) Tensile and compressive stress (σ_{xx}) representation within the 40 Å wide band around the line of dislocations. Positive stress values correspond to compressive and negative stress values corresponds to tensile stress, respectively. b) Average stress above the dislocation cores and c) average stress below the dislocation cores for different hydrogen concentrations [78].

The average dislocation position in the direction of the Burger's vector as a function of time is shown in Figures 2.7a and 2.7b, and in Figure 2.7c and 2.7d, the velocities, respectively, for the ½<111>{110} and ½<111>{112} periodic dislocations. It was observed that the velocity of dislocations decreases with increasing H concentration for both orientation sets, with a strong effect for the 1% H-concentration in the ½<111>{112} dislocation set. Moreover, the point in time when the dislocation started to due to the accumulated shear stress in the initial stages of the shear loading step of the simulations, was delayed by the presence of hydrogen around the dislocation cores. It can be concluded that hydrogen has a pinning effect for both slip systems and that it is more active along the {112} glide plane. In summary, it was found that the presence of hydrogen decreases the velocity of the edge dislocation in α-iron, with the amount depending on the slip system and the dislocation movement regime under consideration. Although the separation distance between the dislocations is stable for both glide planes, the pinning of the ½<111>{112} dislocations is more pronounced for the high hydrogen concentrations.

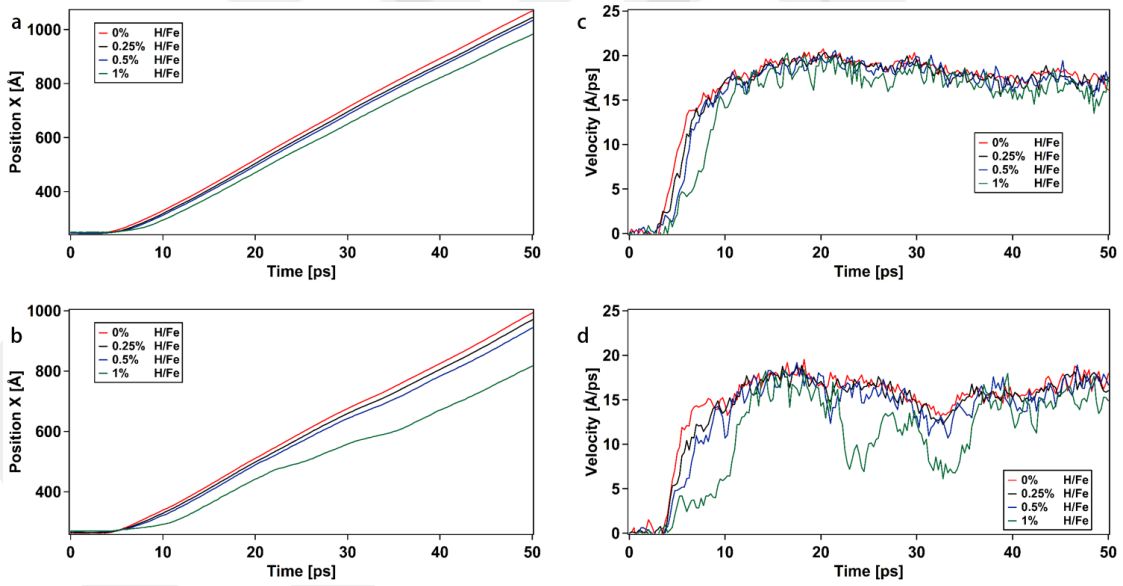

Figure 2.7 Average dislocation position x vs time graph for a) ½<111>{110} and b) ½<111>{112} periodic dislocations. Average instantaneous velocities of c) ½<111>{110} and d) ½<111>{112} periodic dislocations [78].

2.3.2 Grain Boundary – Dislocation Interaction

Figure 2.8 shows the movement of the ½<111>{112} dislocations in the simulation cell containing two grain boundaries for various hydrogen concentrations. Once a single dislocation closely approaches a grain boundary it gets absorbed by the

boundary and requires an additional elastic stress field, e.g., of a subsequent dislocation, to overcome the energy barrier and to continue its movement through the crystal lattice. However, as the hydrogen concentration increases in both the dislocation cores and the grain boundaries, the mobility of the dislocations decreases overall. In the case of no hydrogen (0% H/Fe concentration), after the shear loading, the system stabilizes with two dislocations absorbed in the grain boundaries and with a pair of dislocations stuck behind each grain boundary (Figure 2.8a). Furthermore, after ca. 50 – 70 picoseconds, the accumulation of three dislocations behind the absorbed dislocation builds up a strong enough stress field to nucleate the absorbed dislocation into the crystal on the other side of the grain boundary. However, Figure 2.8b shows that in the presence of 0.25% H/Fe, the elastic stress fields of the dislocations are insufficient to nucleate, and thus re-activate, the dislocation absorbed in the grain boundary. In fact, at higher hydrogen concentrations, more than one dislocation can be absorbed in the grain boundary as shown in the Figures 2.8c and 2.8d. We conclude from these grain boundary + dislocation simulations that hydrogen can increase local plasticity by shielding the elastic long-range interactions between the edge dislocations and other elastic obstacles. This result is consistent with the shielding effect discussed in the context of the HELP mechanism.

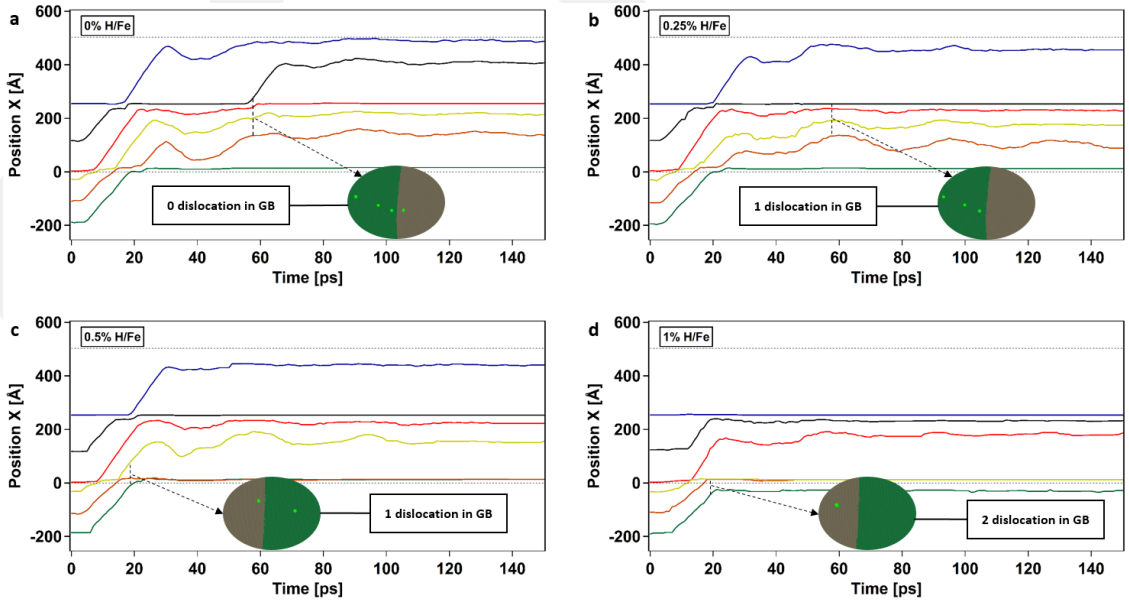

Figure 2.8 X Positions of the single dislocations within the simulation cells containing 2 grain boundaries for a) 0% b) 0.25% c) 0.5% and d) 1% H/Fe concentrations. Grey dots represents the periodic boundaries [78].

2.3.3 Simulations of Tensile Properties

Each of the three supercell orientations mentioned above was exposed to a tensile loading with a constant strain rate and periodic boundaries in all three dimensions in order to evaluate mechanical characteristics and the effect of hydrogen on the pre-existing defects. For the structures without grain boundaries, no fracture was observed up to 50% strain. In contrast, in the supercell containing a grain boundary, intergranular cleavage surfaces were obtained after the deformation-induced grain formation by the same Σ3<110>(112) symmetric tilt grain boundaries.

We first discuss the simulations with single crystals. In the simulations that contained ½<111>{110} dislocations from the outset, all simulation cells showed a similar elastic response and yield stresses were decreased gradually by increasing hydrogen concentration. An immediate softening was observed by yielding with the formation of new dislocations; for increasing H/Fe concentration, the softening process starts earlier, and the pre-existing dislocations showed no mobility for all simulation cells. Tensile stress versus strain graphs are shown in the Figure 2.9.

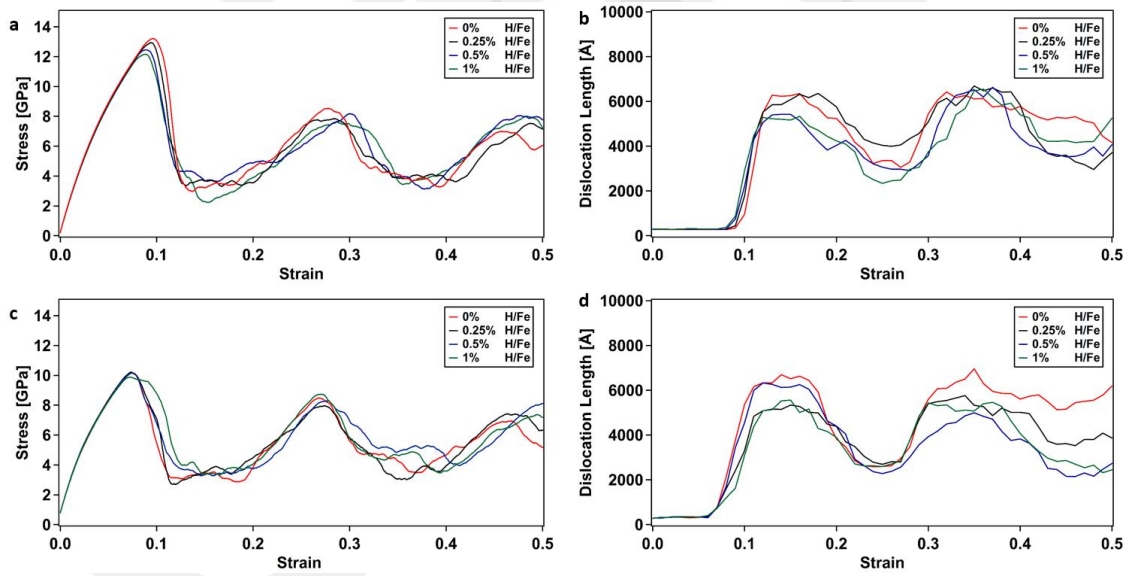

Figure 2.9 Stress and total dislocation length vs strain graphs of the simulation set with ½<111>{110} dislocations, for the single crystal, a,b) for the random initial distribution of the five dislocations, c,d) for the aligned sequence of five dislocations along x axis. Note that the maxima in the dislocation lengths correlate with minima in the stress. Very similar results were observed for the initial distribution with five aligned dislocations and for the initial random distribution: the maximal stress was slightly reduced compared to the random dislocation arrangement, while the strains where the peaks and the minima of the stress and the dislocation lengths occurred were the same [78].

For the simulations with ½<111>{112} dislocations, each configuration showed the same elastic modulus and a hardening stage was observed after yielding with the mobility of pre-existing dislocations (Figure 2.10). Hydrogen was observed to delay and restrict the mobility of the pre-existing dislocations. Also, depending on the hydrogen concentration, dislocations were observed to follow different paths during hardening. In all simulations for the four hydrogen concentrations, the pre-exisiting dislocation mobility was observed along the [-1-11] direction after the yielding that corresponds to the hardening phase. It was also observed that the mobile pre-existing ½<111> dislocations form a junction and nucleate 1<001> dislocations when they encounter each other (Figure 2.11). It was found that the pinning effect of hydrogen on the pre-existing dislocations increases the stress by inhibiting the pre-existing dislocation activity.

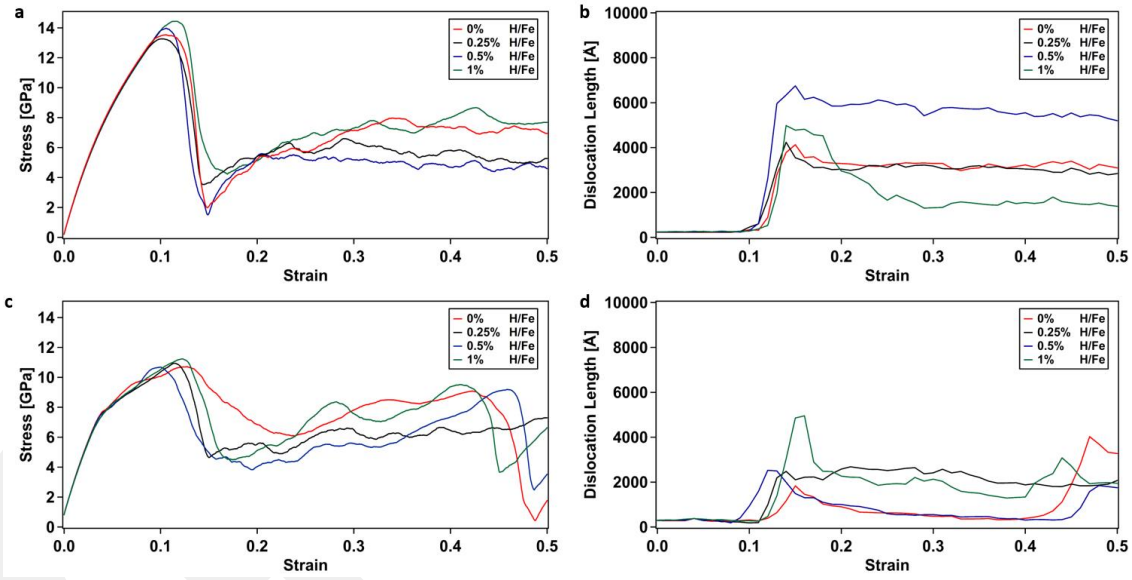

Figure 2.10 Stress and total dislocation length vs strain graphs of the simulation set with ½<111>{112} dislocations, for the single crystal. Again, a,b) are the results found for the random initial distribution of the five dislocations, and c,d) the results for the aligned sequence of five dislocations along the x axis [78].

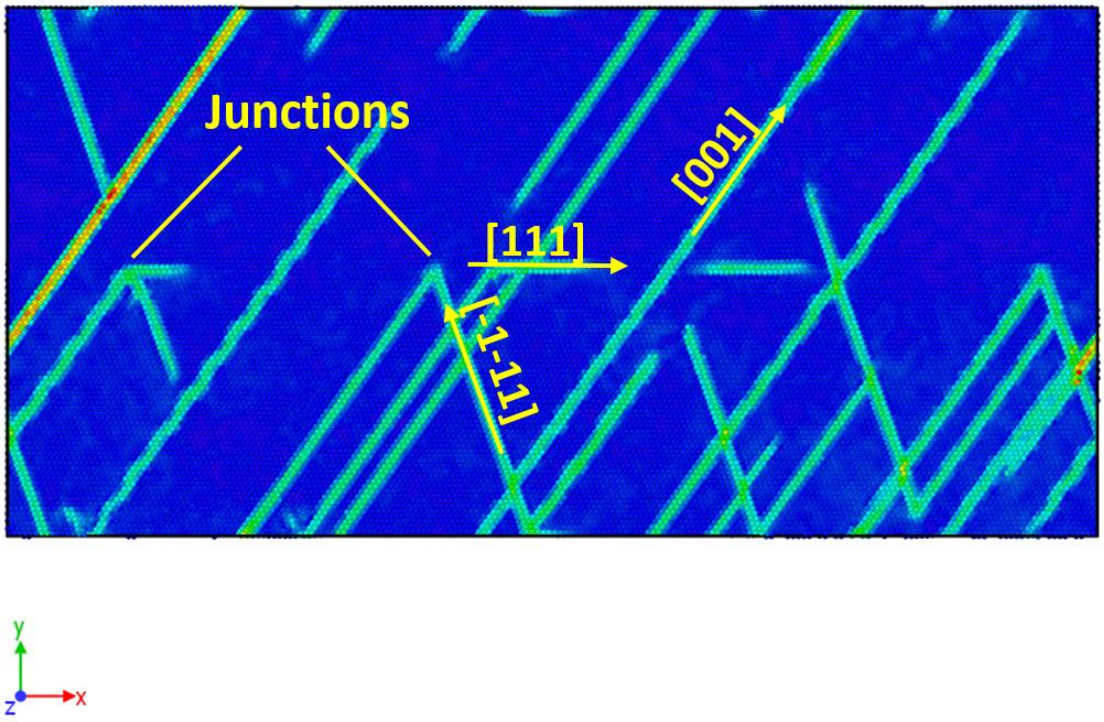

Figure 2.11 Strain paths of pre-existing dislocation in ½<111>{112} dislocation containing supercell after yielding and junction formation, for the single crystal [78].

Turning to the simulations in the presence of grain boundaries, Figure 2.12 shows the stress-strain behaviour for simulation cells containing the two grain boundaries and dislocations, for various hydrogen concentrations. Unlike the single crystal simulations, pre-existing dislocation activity starts immediately after the tensile load was applied in the x direction. For each hydrogen concentration, the pre-existing ½<111>{112} dislocations follow the same path and glide in the <111> direction until every dislocation is absorbed in the grain boundary. Our results reveal that the presence of hydrogen restricts the movement of the dislocations in proportion to the hydrogen concentration and eventually increases the stress for the same strain levels. After that, a softening stage begins with the formation of a new Σ3<110>(112) grain boundary along the [111] direction inside the single crystal part. We observed that the presence of hydrogen inhibits the formation of new grain boundaries and thus, eventually, inside the supercell more stress accumulates during the loading. Figure 2.13 shows the grain configurations for the simulation cells with four different H-concentrations, at the same strain level (7.5%).

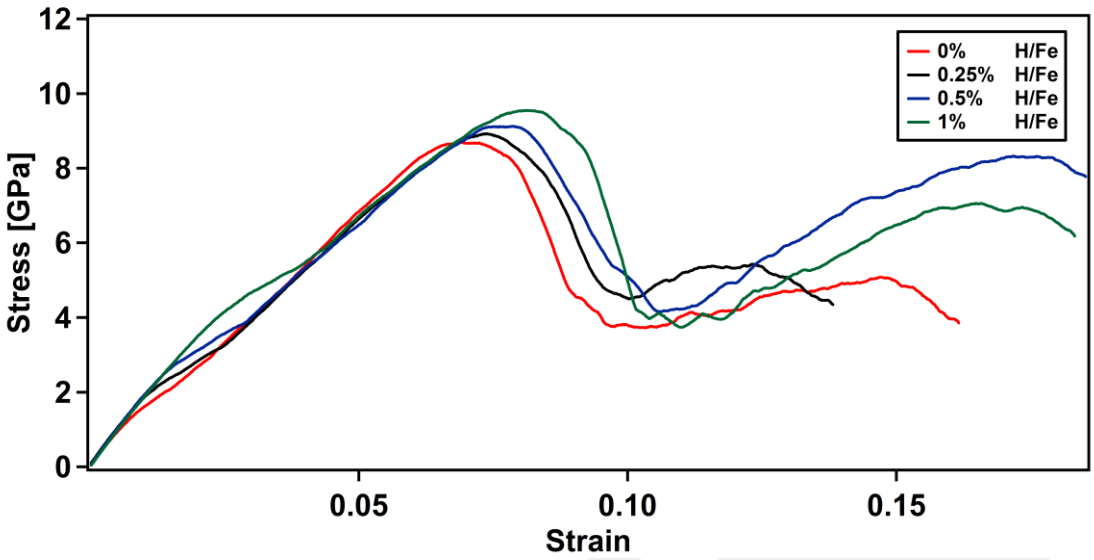

Figure 2.12 Stress and vs strain graphs of the simulation set with grain boundaries and ½<111>{112} dislocations. Note that the softening earlier than for the case without grain boundaries, c.f. Figure 2.9 [78].

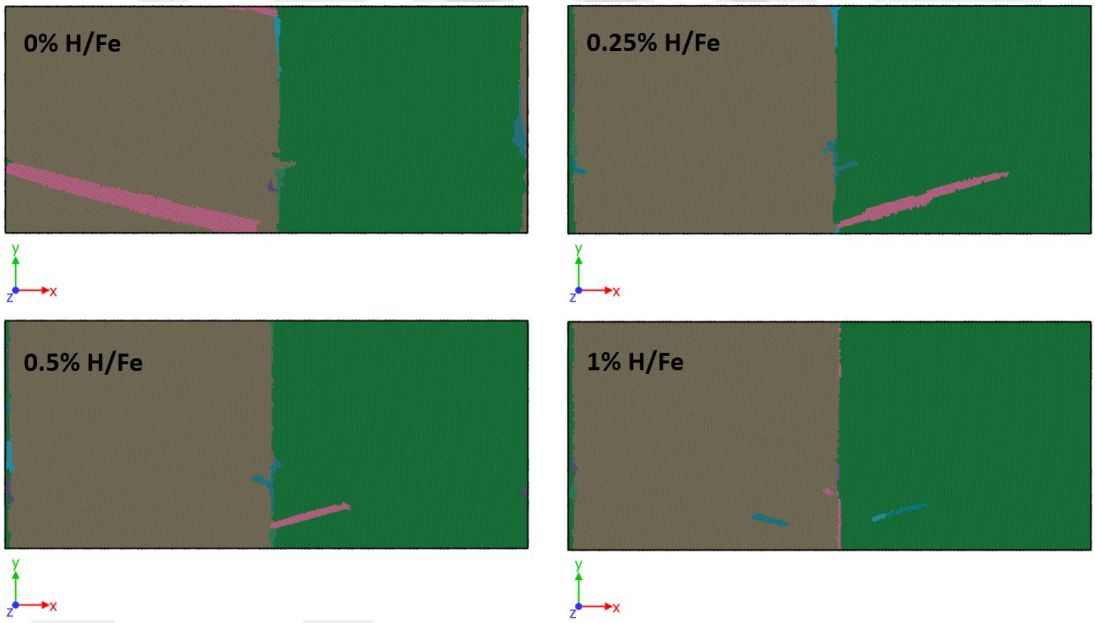

Figure 2.13 Σ3<110>(112) grain boundary formation at 7.5% strain for %0 H/Fe, 0.25% H/Fe, 0.5% H/Fe, and 1% H/Fe supercells. Each colour represents different grains where the newly formed deformation induced grains have the same Σ3<110>(112) grain boundary [78].

2.4 Discussion

During the movement of a dislocation through the crystal lattice, different regimes and mechanisms can play a role depending on the temperature, applied stress, and slip system. At 0 K temperature, an infinitely long dislocation needs to exceed the so-called

Peierls stress in order to start the glide along the Burger's vector direction [79,80]. It is known that the Peierls stress for the ½<111>{112} dislocation is significantly higher than the one for the ½<111>{110} dislocation. Owing to the asymmetrical core structure, the {112} glide plane exhibits different critical stresses depending on the loading direction especially for low temperatures [81]. We note that in one regime, the dislocation movement through the crystal lattice is controlled by the phonon drag dynamics [82]. During the movement of the dislocation, a drag force is acting on the dislocation with a drag coefficient $B(T)$ which depends on the temperature, and the velocity of the dislocation can be expressed as [82,83]

$$v = \frac{\tau b}{B(T)} \quad , \tag{2.5}$$

where τ is the shear stress and b is the magnitude of the Burger's vector. Although several mechanisms contribute to the viscous damping of the dislocation glide, according to this model phonon scattering is the main factor determining the drag coefficient [83,84]. However, atomistic and continuum level studies show that although the phonon drag dynamics is capable of modeling the mobility of the {110} glide plane for appropriate stresses and temperatures, more than one regime should be considered [81–83] when evaluating the behavior in the case of a {112} glide plane. It is also possible for dislocations to move at shears below the Peierls stress when the temperature is high enough to generate thermally activated kink pairs. It was observed in a MD study that the motion of the ½<111>{112} dislocation takes place via nucleation of the kink pairs at temperatures below 100 K, while for higher temperatures the drift of kinks is the dominant process [81]. The velocity of the dislocation that moves by the kink pair formation is defined as [85,86]

$$v_{kp} = \omega_D \frac{bLh}{{x_c}^2} exp\left[\frac{U_{kp}^{(c)}(\tau)}{kT}\right] \tag{2.6}$$

where ω_D is the Debye frequency, $\frac{1}{x_c}$ is the number of possible kink pair formation sites, L is the length of dislocation, h is the periodicity in the barrier, and $U_{kp}^{(c)}(\tau)$ is the kink pair activation energy.

In simulations, for both dislocation types, we observed the formation of kinks while the dislocations glide through the crystal lattice. However, more rapid kink pair formation and reversion, and also gliding as more straight dislocation lines occurred for the {110} glide plane dislocations. On the other hand, {112} glide plane dislocations showed advancement via the nucleation of kink pairs in comparatively higher numbers

and also sustained kink formation for a longer time. These results can also be seen from Figure 2.7: unlike the {110} glide plane dislocation, the average position of the {112} dislocation shows a nonlinear advancement due to the trapped kink pairs which become more distinctive as the hydrogen concentration increases. It was observed from the simulations that when a part of a straight dislocation line encounters a hydrogen-rich region, it gets attracted and trapped within that region with a hydrogen rich medium. Based on this observation, hydrogen was proposed to inhibit the nucleation of new kinks by decreasing the number of kink pair formation sites, and also by reducing the activation energy for the kink pair formation process which is dependent on shear stress. Thus, rather than the drag coefficient being changed by a phonon-impurity scattering, the pinning effect by influencing the kink pair nucleation is observed to be the active mechanism for the reduced mobility of dislocations in the presence of hydrogen. Moreover, although the hydrogen atoms in the core of the dislocations decrease the elastic stress field of the {110} glide plane by more than for the {112} glide plane, the velocity and the total energy around the dislocations was found to decrease by a larger amount for the {112} glide plane than for the {110} dislocation. As a consequence, when there is hydrogen present in the lattice, the pinning effect was observed to be more pronounced for the {112} glide planes, showing an inhibited mobility of the dislocation movement when the dislocation advancement is based on the kink pair nucleation mechanism.

In general, restriction of the movement of the pre-existing {112} dislocations was seen to cause more hardening in the behaviour of the uniaxial tensile stress in addition to a delay in the activity of the pre-existing dislocation until the first maximum in the stress has been reached (Figure 2.10). Although in the single crystal tensile deformation simulations, the dislocations followed different paths, in the initial stage of the grain boundary simulations each dislocation follows the same path and the hardening occurs with increasing hydrogen concentration (Figure 2.12).

Such a hydrogen-induced hardening effect had also been observed in earlier modelling and experimental studies of the pinning role of hydrogen on dislocations movement [87–90]. Unlike the second simulation set with {112} dislocations, structures containing {110} dislocations did not show any dislocation mobility before the emission of new dislocations, since not enough shear stress could accumulate along the <111> direction during tensile loading (Figure 2.9). However, the yield stress was sufficiently reduced by the emission of new dislocations when increasing the hydrogen

concentration. In earlier studies, it had been found that hydrogen can facilitate dislocation emission by decreasing the critical stress intensity at the crack tip [91,92]. From the uniaxial tensile simulations of the single crystalline structures containing pre-existing dislocations, we conclude that hydrogen presence can suppress plasticity and lead to local brittle regions where restriction of the movement of dislocations leads to hardening. On the other hand, we also found that the presence of hydrogen atoms can enhance plasticity by facilitating the emission of new dislocations if there is no pre-existing dislocation activity and plastic behavior occurs via emission of new dislocations.

Movement of the dislocations in the bicrystals with grain boundaries revealed that hydrogen can lead to localization of the regions with enhanced plasticity near elastic obstacles. It was observed from the simulations that the presence of hydrogen decreases the elastic stress fields around the dislocations (Figure 2.6). Furthermore, it was found that in the presence of hydrogen, the transmission of the dislocations across grain boundaries is less likely, due to the reduced elastic field of the sequence of dislocations. Furthermore, a larger energy was required for a dislocation to leave the hydrogen segregated grain boundary. Beside the shielding effect of hydrogen, it was also observed that for a high hydrogen concentration (1% H/Fe), the grain boundary can absorb more than one dislocation, while only one dislocation can be absorbed and emitted at a time for the lower hydrogen concentrations (Figure 2.8). In earlier investigations of Ni and Fe symmetric tilt grain boundaries and screw dislocations interactions, it had been observed that when the hydrogen segregates along the grain boundaries, this can increase the energy barrier for the dislocation-GB interactions such as transmission, absorption, and emission [93,94]. Additionally, tensile simulations of the bicrystals reveal that strain-induced grain nucleation was suppressed by the increasing hydrogen concentration. For the same strains, we observed grain formations in various volumes depending on the hydrogen concentration (Figure 2.13). Furthermore, in previous molecular dynamics studies on the bcc Fe nanograins, it was found that hydrogen can inhibit the GB-related deformation processes such as grain boundary migration, rotation, sliding, and also dislocation and deformation twin nucleation from the grain boundary due to the grain boundary disorder and reduced mobility of the grain boundaries which eventually suppress the plastic deformation [65,95]. Finally, from the simulations, we can conclude that hydrogen can facilitate the existence of local brittle

fracture points around the grain boundary by suppressing the strain-induced grain nucleation.

2.5 Conclusion

In summary, we investigated the role of hydrogen on the edge dislocation mobility and also grain boundary-dislocation interactions in alpha-iron. To further evaluate these systems, uniaxial tensile loadings were performed under constant strain rate. The following conclusions can be drawn from the study;

(1) The presence of hydrogen in the crystal lattice decreases the velocity of the edge dislocations and the movement regime is a determining factor regarding the magnitude of the reduced mobility. It was observed that the pinning effect of the hydrogen atoms on the dislocation is more pronounced when the glide occurs via kink pair formation.

(2) When the dislocations encounter an elastic obstacle, hydrogen can shield the elastic stress fields between dislocation pile ups and it can facilitate plasticity localization as suggested in the HELP mechanism. Moreover, the energy required for dislocation transmission across the grain boundary is higher in the presence of hydrogen, which can lead to enhanced plastic behavior around the grain boundary.

(3) While the pre-existing dislocations are mobile in the single crystal and bicrystal, hardening was observed, suggesting the pinning effect of the hydrogen atoms as the mechanism. Although this can lead to inhibition of plasticity and formation of brittle crack initiation points, it was also shown that hydrogen presence can decrease the required stress for emission of dislocations and actually enhance local plasticity.

(4) Atomic configuration disorder at the grain boundary by segregated hydrogen can contribute to the plasticity localization by increasing defect absorption. However, brittle behavior was also observed in bicrystals by the reduction of strain-induced grain nucleation capacity under the effect of hydrogen.

Chapter 3

3. Investigation of Hydrogen Diffusion Profile of Different Metallic Materials for a Better Understanding of Hydrogen Embrittlement

3.1 Introduction

One key factor on the hydrogen embrittlement susceptibility of the metallic materials is the diffusivity of the hydrogen in the crystal lattice. It is known that close-packed structures possess a lower hydrogen diffusivity compared to less dense materials. Considering the high strength steels, hydrogen has a lower diffusivity in austenite (fcc) or deformation induced ε-martensite (hcp) than ferrites (bcc). Determination of the hydrogen diffusivity is conducted by hydrogen diffusion coefficient calculations in materials. Many ab-initio simulations were performed so far to determine the diffusion coefficient of hydrogen in different crystal structures. In first-principle studies, it was found that diffusion coefficient of the hydrogen in the three different crystals of the iron structure can be sorted as $D_{\alpha-Fe} > D_{\gamma-Fe} > D_{\varepsilon-Fe}$ [96,97].

In bcc iron, ab-initio studies show that hydrogen atoms mostly occupy tetrahedral sites in the crystal whereas in high concentration regions occupation of octahedral sites can be observed [98,99]. Usually, diffusion in the lattice takes place via the migration of the hydrogen from tetrahedral site to the nearest tetrahedral site by classical overbarrier jump migration [96–100]. In the fcc nickel, octahedral sites are the favorable hydrogen occupation sites and indirect diffusion occur through a metastable tetrahedral site between two octahedral sites [100,101]. Theoretical studies on the preferable sites of the hydrogen in hcp titanium show that octahedral sites are more stable whereas previous experimental works indicates that the tetrahedral sites are more stable [102]. Thus, evaluating the diffusion of the hydrogen in hcp titanium requires to consider O-O, T-T,

O-T energy barriers for hydrogen to migrate along lattice [103]. Investigating the hydrogen diffusion in these three crystal structures is important for understanding the susceptibility to hydrogen of the materials and alloys that includes the same crystal types. Additionally, many experimental studies conducted so far to understand the effect of hydrogen on the materials by introducing the hydrogen into material microstructure either by pressurized gaseous hydrogen or cathodic charging of the specimens. In the cathodic hydrogen charging, both specimen and an anode is submerged into an electrolytic solution where H+ accumulates on the specimen surface with the flux produced by the potential applied to the system [104]. This is a widely used method to evaluate the mechanical properties of the materials e.g. tensile, fatigue, fracture toughness and, impact properties after the introduction of the hydrogen into the microstructure [41,105–107]. However, it is crucial to understand the hydrogen content and distribution in the specimens depending on the charging time, temperature and also hydrogen diffusivity of the materials. Thus, modelling the hydrogen concentration in the materials by these parameters is significant to understand the effect of the hydrogen during experimental testing and also to evaluate the susceptibility of materials to hydrogen embrittlement. Additionally, removal of the hydrogen and preventing the hydrogen embrittlement can be accomplished by baking of the specimens under certain temperatures and baking times [108,109]. Thus, modelling the concentration profile of the hydrogen charged materials subsequent to a discharge can enable to specify the required baking times and temperatures to prevent the hydrogen embrittlement.

In this study, 1D and 2D transient diffusion profiles of the hydrogen were investigated in bcc iron, fcc nickel, and hcp titanium by utilizing numerical models in MATLAB. Diffusion coefficients for the three types of materials were utilized in the material model with different temperatures. Analyses were performed with different charging times and corresponding hydrogen concentrations were observed. Additionally, back-diffusion of the hydrogen from the material surfaces was also evaluated by the effect of temperature and the concentration change along the charged materials were observed for different baking times.

3.2 Methodology

In order to define the hydrogen diffusion model for three material types, Fick’s second law of diffusion and a numerical diffusion equations were used for 1D and 2D

mediums respectively. Diffusion analysis were performed by MATLAB both for 1D and 2D transient models. Each model was utilized for iron, nickel, and titanium elements with bcc, fcc, and hcp crystal structures respectively. For the 1D diffusion model, normalized concentration value at the position x is defined according to Fick's second law of diffusion [110];

$$\frac{C(x)-C_s}{C_s-C_0} = 1 - \mathrm{erf}\left(\frac{x}{2\sqrt{Dt}}\right) \quad \textbf{(3.1)}$$

Where $C(x)$ is the concentration at point x, C_s concentration at boundary, C_0 initial concentration and D is the diffusion coefficient of the specific crystal when no hydrogen trap is considered. According to Arrhenius equation D can be defined as;

$$D = D_0 exp\left[-\frac{E_a}{k_B T}\right] \quad \textbf{(3.2)}$$

Where D_0 is pre-exponential factor and E_a is the activation energy of the hydrogen diffusion. Diffusion coefficient of the hydrogen in a single crystal can also be defined by the transition state theory [96,97];

$$D = nL^2 \frac{k_B T}{h} exp\left[-\frac{E_a}{k_B T}\right] \quad \textbf{(3.3)}$$

where the n is a numerical coefficient, L is the distance between the two neighboring stable position of hydrogen in the crystal e.g. in bcc crystals nearest tetrahedral sites where the hydrogen atoms can reside and h is the Planck's constant. Table 1 represents the diffusion coefficients used in the study for the three types of materials at applied temperatures [111].

Table 3.1. Diffusion coeffecients of Fe, Ni, and Ti used in the study at 25 °C, 80 °C, and 100 °C temperatures [111]**.**

Material	D (m^2s^{-1}), 25 °C	D (m^2s^{-1}), 80 °C	D (m^2s^{-1}), 100 °C
Iron	2.5035×10^{-9}	2.9845×10^{-9}	3.1925×10^{-9}
Nickel	9.3296×10^{-13}	2.0007×10^{-12}	2.6342×10^{-12}
Titanium	4.2183×10^{-13}	8.7690×10^{-13}	1.1371×10^{-12}

In the 1D diffusion model (eq.1), hydrogen concentration profiles were calculated by the diffusion coefficients at 25 °C and 80 °C temperatures. For each material the concentration in 5 mm depth was calculated after the 1, 8, 24, and 72 hours of charging.

Subsequently, a transient numerical diffusion model was utilized to obtain hydrogen concentration in a 2D 10 mm x 10 mm medium. Considering the hydrogen concentration $C_{x,y,t}$ in a 2D cartesian coordinate system in position x, y and in time t, the rate of the concentration change with respect to time can be defined as;

$$\frac{C_{x,y,t}}{\partial t} = D\left[\frac{\partial^2 C_{x,y,t}}{\partial^2 x^2} + \frac{\partial^2 C_{x,y,t}}{\partial^2 y^2}\right] \quad \textbf{(3.4)}$$

The subsequent concentration in the position after a time increment can be found by;

$$C_{x,y,t+1} = C_{x,y,t} + d\left[C_{x+1,y,t} + C_{x-1,y,t} + C_{x,y+1,t} + C_{x,y-1,t} - 4C_{x,y,t}\right] \quad \textbf{(3.5)}$$

where the d is defined as;

$$d = D\frac{\Delta t}{\Delta x^2} \quad \textbf{(3.6)}$$

Calculations of the 2D transient model were utilized by the eq.5 and eq.6 in a 10 mm x 10 mm medium where the initial hydrogen concentration $C_0 = 0$ and the surface concentration $C_s = 1$ for different time intervals.

Finally, back diffusion of the hydrogen under the 100 °C temperature was modelled after the 24 hours charging of each material types without the hydrogen concentration along surfaces.

3.3 Results & Discussion

1D hydrogen diffusion profiles of the iron, nickel, and titanium in a 5 mm depth were shown in the figure 1 for different charging times. Only in bcc Fe hydrogen was observed through total depth for all charging times due to the high diffusion coefficient of the hydrogen in bcc structures (figure 1a). However, in nickel (fcc) and titanium (hcp) lattices, hydrogen presence was not observed along the total length for each charging times. Increase in the hydrogen concentration by the effect of temperature was also observed for the same charging times.

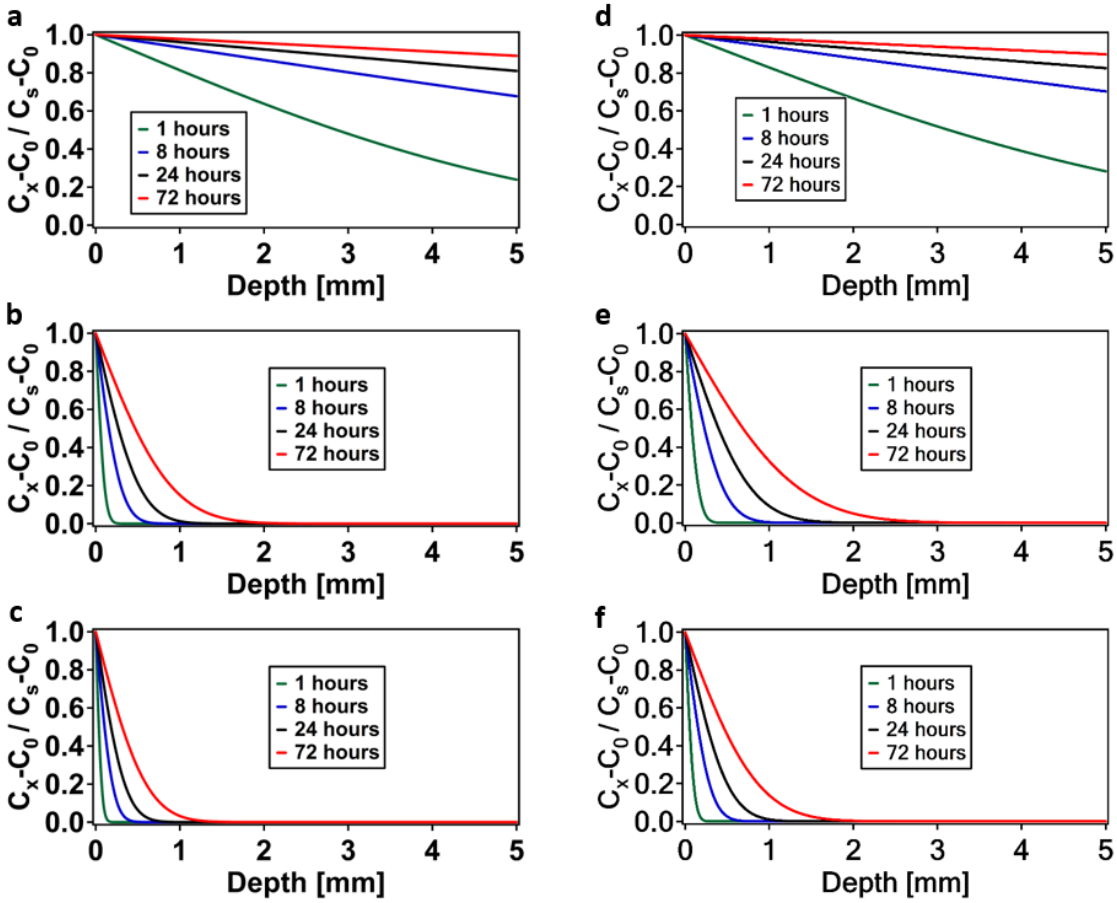

Figure 3.1 1D diffusion profiles of the a) Fe b) Ni c) Ti at 25 °C and d) Fe e) Ni f) Ti at 80 °C for 1, 8, 16 and, 72 hours charging times.

2D diffusion profiles of the hydrogen in the materials are shown in the figure 2. Due to the natural symmetry of the system only the diffusion through x axis was illustrated at y = 5. Compared to 1D diffusion model with the Fick's second law of equation, bcc iron showed a larger difference on the amount of hydrogen diffused into system. Indeed, concentration gap between the 1D and 2D models was more distinctive in the bcc iron with a higher diffusion coefficient since the hydrogen diffusion through y axis reaches to 5 mm in all charging times.

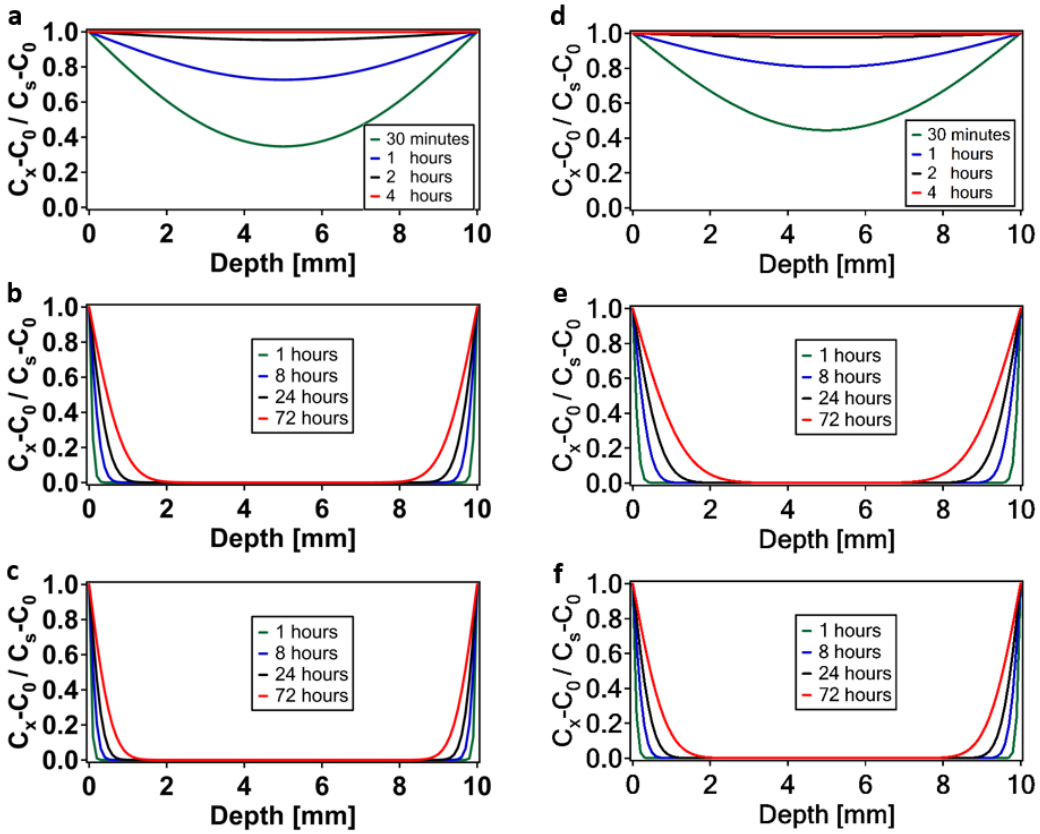

Figure 3.2. 2D diffusion profile of the hydrogen along x direction (y=5) into a) Fe b) Ni and c) Ti at 25 °C and d) Fe e) Ni and f) Ti at 80 °C.

Both 1D and 2D results revealed that concentration profile after hydrogen charging is dependent on the material type, temperature, and also charging time. In bcc iron, it was observed that hydrogen concentration in the material was equilibrated with the surface concentration after 2 hours of charging. However, fcc nickel and hcp titanium lattices showed that even after 72 hours of charging no hydrogen concentration can be observed in the center of the specimen and the hydrogen permeation is limited with 2 mm depth subsurface region. Thus, crystal structure type was observed as the determinant parameter on the diffusion of the hydrogen and materials with bcc crystal structure type are the most susceptible to hydrogen diffusion. In an experimental study on the diffusion profile of β-titanium (bcc) alloy, it was observed from the numerical calculations for a radial specimen that after 10 minutes of charging hydrogen concentration was equilibrated with the surface along 1 mm depth under 500 °C temperature [112]. The effect of the hydrogen in the microstructure can also be observed by transition in the failure mode i.e. ductile failure to brittle failure of materials. Thus, investigation of the fracture surfaces of the hydrogen charged specimens can indicate the hydrogen diffused regions in the microstructure. In an

experimental study, from fracture surface of the cathodic hydrogen charged fcc nickel based alloy, 135 μm and 300 μm depth brittle zone was observed after 1 hours and 5 hours of hydrogen charging respectively [113]. Additionally, TDS (Thermal Desorption Analysis) is a widely used method to understand the hydrogen accumulated within the materials. Hydrogen atoms can reside in interstitial positions or can be trapped in the defects sites e.g. grain boundaries, dislocations, and vacancies with different binding energies. Hydrogen desorption flux thorough the surface of the material can be observed by TDS method by increasing temperature where the flux shows a peak when the trapped hydrogen inside the defect have enough energy to overcome binding energy [114]. In an experimental TDS analysis that investigate the pure iron and nickel alloy hydrogen desorption content under tensile loading, highest amount of hydrogen desorption was observed in bcc iron due to the higher diffusion coefficient [115].

One prevention method of the mechanical degradation effect of the hydrogen is the back diffusion of the hydrogen from the surface by the effect of temperature. However, in order to specify the ideal time and the temperature it is required to understand the hydrogen content in the material and also diffusivity of hydrogen. Results of the hydrogen back diffusion simulations for 24 hours charged materials were shown in the figure 3. Remaining hydrogen concentration after the baking operations, also change in the hydrogen concentration after back diffusion of hydrogen under 100 °C temperature was illustrated for different baking times. Results revealed that most hydrogen concentration was accumulated in the middle of the hydrogen charged region. Since the hydrogen concentration was equilibrated with the surface concentration after charging in bcc iron, the peak hydrogen content and the least hydrogen concentration change was observed in the middle of the simulation area. On the other hand, after the baking, the mass center of the hydrogen concentration was located at the subsurface for nickel and titanium lattice. During the back-diffusion hydrogen was observed to permeate both through surface and through center of the medium. Thus, although the fcc and hcp structures have a less hydrogen diffusivity compared to bcc, back-diffusion of the hydrogen requires larger charging times and higher baking temperatures. An experimental study on the different baking temperatures and times of martensitic steel revealed that although the baking under 100 °C temperature showed a slight hydrogen desorption difference for different baking times, under 150 °C and 200 °C temperatures with minimum 20 minutes of baking, HE susceptibility can be eliminated for the martensitic steel [116]. Additionally, in an experimental study of gaseous charged

austenitic steel, 48 hours baking of the specimen under 160 °C temperature was found to eliminate the embrittlement effect of the hydrogen due to the removal from the surface despite the hydrogen presence inside the material [117]. Our results also showed that the most reduction in the hydrogen concentration occurred at the surface in fcc and other crystal structures as well.

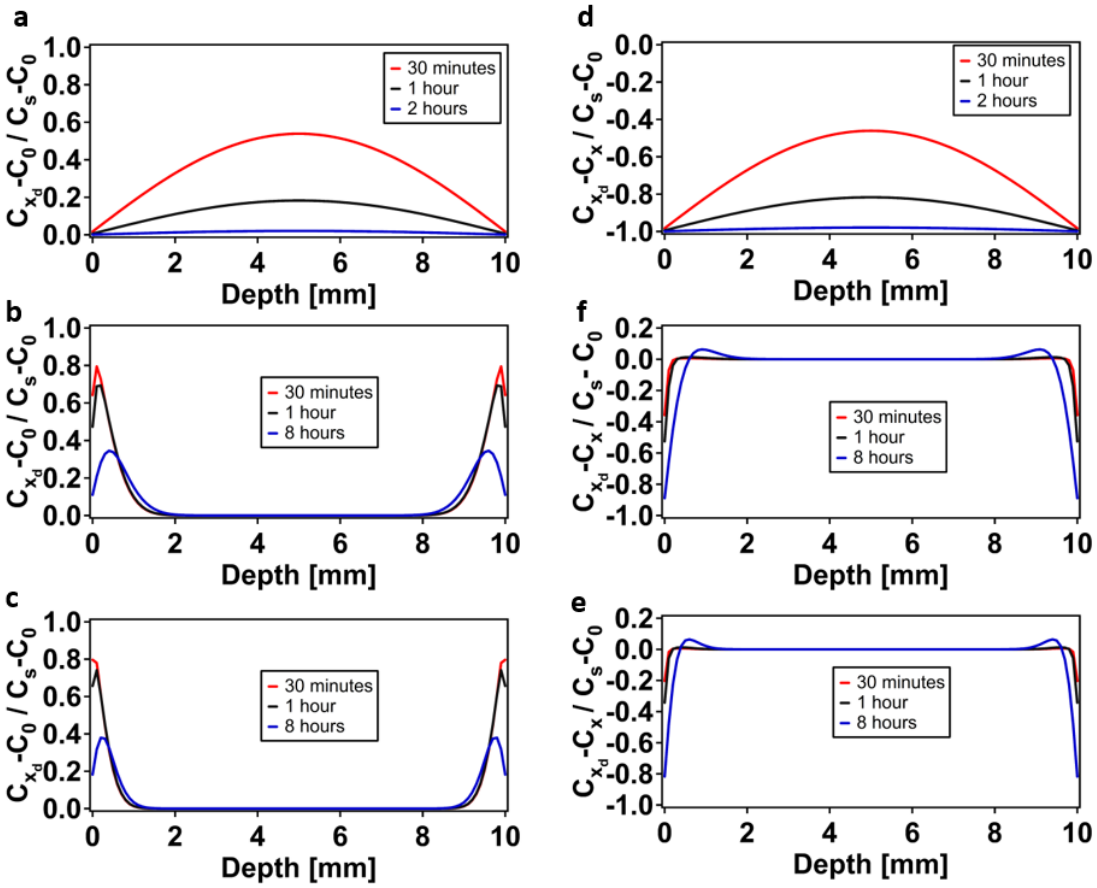

Figure 3.3. Remaining hydrogen concentration after the back diffusion for a) Fe b) Ni c) Ti and normalized hydrogen concentration with initial hydrogen concentration for d) Fe e) Ni and f) Ti.

3.3 Conclusion

In this study, 1D and 2D transient hydrogen diffusion profiles of iron, nickel, and titanium crystals were investigated with bcc, fcc, and hcp crystal structures respectively. Results revealed that hydrogen concentration is dependent on the crystal structure, temperature, and hydrogen exposure times of the materials. Back-diffusion of the hydrogen was modelled for each material under certain baking temperature. Results showed that although the hydrogen diffusion susceptibility of bcc crystal is higher

compared to the fcc and hcp structures. Back-diffusion of the hydrogen in these crystals requires larger baking times and higher temperatures.

Chapter 4

4. Conclusions and Future Prospects

4.1 Conclusions

In this thesis, hydrogen diffusion and hydrogen defect interactions as well as the influences of these interactions on the mechanical response were evaluated by a multi-scale method. Detrimental effects of the hydrogen on the metallic materials were known for a long period of time. Unveiling these effects requires modeling the metal and hydrogen interactions in both macroscopic and atomistic scales. The concentration of the hydrogen around the defects was investigated by both utilizing continuum level theoretical and atomistic approaches. Furthermore, dislocation mobility in the single crystal and transmission of the dislocation across a grain boundary were evaluated in the presence of hydrogen. The influence of the dislocation mobility on the mechanical response was also evaluated in addition to the deformation behavior of the bicrystal under uniaxial stress. Finally, numerical modelling of the hydrogen diffusion into bcc, fcc, and hcp crystal structures were conducted in order to observe the HE susceptibility of the materials followed by hydrogen back diffusion analysis as well. Results revealed that hydrogen inhibits the mobility of the edge dislocations in bcc iron that induce a hardening response during the pre-existing dislocation activity. Additionally, in the case that plasticity occurs via emission of the new dislocation, hydrogen facilitates the new dislocation emission and causes an earlier softening under loading. Moreover, it was observed that hydrogen inhibits the nucleation of the new grains that can lead formation of brittle fracture points in the materials. Finally, it was observed from the hydrogen diffusion simulations that although more hydrogen accumulation was observed in the bcc crystals for the same conditions, fcc and hcp containing materials requires higher baking times and temperatures in order to remove the hydrogen and to prevent the hydrogen embrittlement.

4.2 Societal Impact and Contribution to Global Sustainability

Hydrogen energy stands as a promising clean and sustainable energy source and attracting attention gradually while fossil fuels are being endeavored to replace with new alternatives [118,119]. Additionally, the use of hydrogen as an energy source has a high potential on the solution of energy shortage, pollution arising from fossil fuel usage, and also economic cost of currently used energy sources. When the hydrogen used in the fuel cells only water is being produced at the end of the energy generation process. Also, hydrogen is the most abundant element in the universe and it can be obtained by other clean energy technologies such as wind power solar power. After the hydrogen is produced, it can be stored and transported for any energy required application. However, there are key issues to be overcome to use hydrogen in stationary and on-board applications. Thus, the development of new hydrogen storage technologies is crucial to construct such a hydrogen economy for the future.

One of the most important challenges is the transportation and storage of hydrogen [120–122]. Due to the small size, atomic hydrogen is very prone to diffuse into metallic materials, and interaction of the hydrogen with crystal defects can cause degradation of mechanical properties a phenomenon known as hydrogen embrittlement. In this thesis, atomic mechanisms of hydrogen-defect interactions were investigated in order to understand the hydrogen embrittlement phenomena. Although there are many studies in the literature, the exact mechanism of hydrogen induced degradation of metals is still unclear. Many factors such as hydrogen content in the environment and the load exposure of the material can contribute to ultimate results. However, the most important factor can be considered as the behaviour of the hydrogen in the microstructure and interaction with crystal defects. Thus, revealing the underlying mechanism can provide to develop new metallic materials to be used in the storage and transportation of hydrogen.

4.3 Future Prospects

In the thesis, mostly the effect of the hydrogen on the long range interactions of defects and mechanical behavior of defect containing structures were examined by an

interatomic potential from the literature. However, for the future prospect hydrogen diffusion mechanisms and interaction with defects will be studied in detail by ab-initio calculations. Furthermore, the nano-scale outputs of the study with current molecular dynamics results e.g. dislocation velocity will be used as input in the continuum and FEM models in order to obtain a more comprehensive multi-scale model for the hydrogen embrittlement.

BIBLIOGRAPHY

[1] B. Bal, I. Sahin, A. Uzun, D. Canadinc, A New Venue Toward Predicting the Role of Hydrogen Embrittlement on Metallic Materials, Metall. Mater. Trans. A Phys. Metall. Mater. Sci. 47 (2016) 5409–5422. doi:10.1007/s11661-016-3708-z.

[2] S.P. Lynch, Environmentally assisted cracking: Overview of evidence for an adsorption-induced localised-slip process, Acta Metall. 36 (1988) 2639–2661. doi:10.1016/0001-6160(88)90113-7.

[3] M.A. V. Devanathan, Z. Stachurski, W. Beck, A Technique for the Evaluation of Hydrogen Embrittlement Characteristics of Electroplating Baths, J. Electrochem. Soc. 110 (1963) 886. doi:10.1149/1.2425894.

[4] M.A. Arafin, J.A. Szpunar, Effect of bainitic microstructure on the susceptibility of pipeline steels to hydrogen induced cracking, Mater. Sci. Eng. A. 528 (2011) 4927–4940. doi:10.1016/j.msea.2011.03.036.

[5] D. V. Edmonds, R.C. Cochrane, Structure-property relationships in bainitic steels, Metall. Trans. A. 21 (1990) 1527–1540. doi:10.1007/BF02672567.

[6] J. Zheng, X. Liu, P. Xu, P. Liu, Y. Zhao, J. Yang, Development of high pressure gaseous hydrogen storage technologies, Int. J. Hydrogen Energy. 37 (2012) 1048–1057. doi:10.1016/j.ijhydene.2011.02.125.

[7] A. Barnoush, Hydrogen embrittlement revisited by in situ electrochemical nanoindentation, Saarland University (2007).

[8] H. Peisl, Lattice strains due to hydrogen in metals, Springer Berlin Heidelberg (1978): 53–74. doi:10.1007/3540087052_42.

[9] M. Stashchuk, M. Dorosh, Evaluation of hydrogen stresses in metal and redistribution of hydrogen around crack-like defects, Int. J. Hydrogen Energy. 37 (2012) 14687–14696. doi:10.1016/j.ijhydene.2012.07.093.

[10] S. Yang, S.H. Yun, T. Oda, Molecular dynamics simulation on stability and diffusivity of hydrogen around a <111> symmetric tilt grain boundary in bcc-Fe, Fusion Eng. Des. 131 (2018) 105–110. doi:10.1016/j.fusengdes.2018.04.092.

[11] S. Lynch, Hydrogen embrittlement phenomena and mechanisms, Corros. Rev. 30 (2012) 105–123. doi:10.1515/corrrev-2012-0502.

[12] L.B. Pfeil, P.R.S.L. A, The effect of occluded hydrogen on the tensile strength of iron, Proc. R. Soc. London. Ser. A, Contain. Pap. a Math. Phys. Character. 112 (1926) 182–195. doi:10.1098/rspa.1926.0103.

[13] Z. Tarzimoghadam, M. Rohwerder, S. V. Merzlikin, A. Bashir, L. Yedra, S. Eswara, D. Ponge, D. Raabe, Multi-scale and spatially resolved hydrogen mapping in a Ni-Nb model alloy reveals the role of the δ phase in hydrogen embrittlement of alloy 718, Acta Mater. 109 (2016) 69–81. doi:10.1016/j.actamat.2016.02.053.

[14] Y. Katz, N. Tymiak, W.W. Gerberich, Nanomechanical probes as new approaches to hydrogen/deformation interaction studies, Eng. Fract. Mech. 68 (2001) 619–646. doi:10.1016/S0013-7944(00)00119-3.

[15] A.G. Varias, A.R. Massih, Hydride-induced embrittlement and fracture in metals - Effect of stress and temperature distribution, J. Mech. Phys. Solids. 50 (2002) 1469–1510. doi:10.1016/S0022-5096(01)00117-X.

[16] C.L. Briant, Z.F. Wang, N. Chollocoop, Hydrogen embrittlement of commercial

purity titanium, Corros. Sci. 44 (2002) 1875–1888. doi:10.1016/S0010-938X(01)00159-7.
[17] Y. Udagawa, M. Yamaguchi, H. Abe, N. Sekimura, T. Fuketa, Ab initio study on plane defects in zirconium-hydrogen solid solution and zirconium hydride, Acta Mater. 58 (2010) 3927–3938. doi:10.1016/j.actamat.2010.03.034.
[18] P. Sofronis, Y. Liang, N. Aravas, Hydrogen induced shear localization of the plastic flow in metals and alloys, Eur. J. Mech. A/Solids. 20 (2001) 857–872. doi:10.1016/S0997-7538(01)01179-2.
[19] T. Depover, K. Verbeken, The detrimental effect of hydrogen at dislocations on the hydrogen embrittlement susceptibility of Fe-C-X alloys: An experimental proof of the HELP mechanism, Int. J. Hydrogen Energy. 43 (2018) 3050–3061. doi:10.1016/j.ijhydene.2017.12.109.
[20] M. Koyama, C.C. Tasan, E. Akiyama, K. Tsuzaki, D. Raabe, Hydrogen-assisted decohesion and localized plasticity in dual-phase steel, Acta Mater. 70 (2014) 174–187. doi:10.1016/j.actamat.2014.01.048.
[21] Y.S. Chen, D. Haley, S.S.A. Gerstl, A.J. London, F. Sweeney, R.A. Wepf, W.M. Rainforth, P.A.J. Bagot, M.P. Moody, Direct observation of individual hydrogen atoms at trapping sites in a ferritic steel, Science (80-.). 355 (2017) 1196–1199. doi:10.1126/science.aal2418.
[22] T. Magnin, A. Chambreuil, B. Bayle, The corrosion-enhanced plasticity model for stress corrosion cracking in ductile fcc alloys, Acta Mater. 44 (1996) 1457–1470. doi:10.1016/1359-6454(95)00301-0.
[23] D. Pérez Escobar, T. Depover, L. Duprez, K. Verbeken, M. Verhaege, Combined thermal desorption spectroscopy, differential scanning calorimetry, scanning electron microscopy and X-ray diffraction study of hydrogen trapping in cold deformed TRIP steel, Acta Mater. 60 (2012) 2593–2605. doi:10.1016/j.actamat.2012.01.026.
[24] Y. Zhao, D.H. Lee, M.Y. Seok, J.A. Lee, M.P. Phaniraj, J.Y. Suh, H.Y. Ha, J.Y. Kim, U. Ramamurty, J. il Jang, Resistance of CoCrFeMnNi high-entropy alloy to gaseous hydrogen embrittlement, Scr. Mater. 135 (2017) 54–58. doi:10.1016/j.scriptamat.2017.03.029.
[25] O. Barrera, E. Tarleton, H.W. Tang, A.C.F. Cocks, Modelling the coupling between hydrogen diffusion and the mechanical behaviour of metals, Comput. Mater. Sci. 122 (2016) 219–228. doi:10.1016/j.commatsci.2016.05.030.
[26] P. Sofronis, R.M. McMeeking, Numerical analysis of hydrogen transport near a blunting crack tip, J. Mech. Phys. Solids. 37 (1989) 317–350. doi:10.1016/0022-5096(89)90002-1.
[27] A. Ramasubramaniam, M. Itakura, E.A. Carter, Interatomic potentials for hydrogen in α -iron based on density functional theory, Phys. Rev. B - Condens. Matter Mater. Phys. 79 (2009) 1–13. doi:10.1103/PhysRevB.79.174101.
[28] M. Wen, X.J. Xu, S. Fukuyama, K. Yokogawa, Embedded-atom-method functions for the body-centered-cubic iron and hydrogen, J. Mater. Res. 16 (2001) 3496–3502. doi:10.1557/JMR.2001.0480.
[29] B.J. Lee, J.W. Jang, A modified embedded-atom method interatomic potential for the Fe-H system, Acta Mater. 55 (2007) 6779–6788. doi:10.1016/j.actamat.2007.08.041.
[30] P. Kuopanportti, E. Hayward, C.C. Fu, A. Kuronen, K. Nordlund, Interatomic Fe-H potential for irradiation and embrittlement simulations, Comput. Mater. Sci. 111 (2016) 525–531. doi:10.1016/j.commatsci.2015.09.021.
[31] W.H. Johnson, II. On some remarkable changes produced in iron and steel by the

action of hydrogen and acids, Proc. R. Soc. London. 23 (1875) 168–179. doi:10.1098/rspl.1874.0024.
[32] J. Woodtli, R. Kieselbach, Damage due to hydrogen embrittlement and stress corrosion cracking, Eng. Fail. Anal. 7 (2000) 427–450. doi:10.1016/S1350-6307(99)00033-3.
[33] D. Hardie, E.A. Charles, A.H. Lopez, Hydrogen embrittlement of high strength pipeline steels, Corros. Sci. 48 (2006) 4378–4385. doi:10.1016/j.corsci.2006.02.011.
[34] R.A. Oriani, Hydrogen Embrittlement of Steels, Annu. Rev. Mater. Sci. 8 (1978) 327–357. doi:10.1146/annurev.ms.08.080178.001551.
[35] M. Koyama, E. Akiyama, Y.K. Lee, D. Raabe, K. Tsuzaki, Overview of hydrogen embrittlement in high-Mn steels, Int. J. Hydrogen Energy. 42 (2017) 12706–12723. doi:10.1016/j.ijhydene.2017.02.214.
[36] R.G. Song, W. Dietzel, B.J. Zhang, W.J. Liu, M.K. Tseng, A. Atrens, Stress corrosion cracking and hydrogen embrittlement of an Al-Zn-Mg-Cu alloy, Acta Mater. 52 (2004) 4727–4743. doi:10.1016/j.actamat.2004.06.023.
[37] B. Bal, M. Koyama, G. Gerstein, H.J. Maier, K. Tsuzaki, Effect of strain rate on hydrogen embrittlement susceptibility of twinning-induced plasticity steel pre-charged with high-pressure hydrogen gas, Int. J. Hydrogen Energy. 41 (2016) 15362–15372. doi:10.1016/j.ijhydene.2016.06.259.
[38] H. Najam, M. Koyama, B. Bal, E. Akiyama, K. Tsuzaki, Strain rate and hydrogen effects on crack growth from a notch in a Fe-high-Mn steel containing 1.1 wt% solute carbon, Int. J. Hydrogen Energy. 45 (2020) 1125–1139. doi:10.1016/j.ijhydene.2019.10.227.
[39] Z. Zhang, G. Obasis, R. Morana, M. Preuss, Hydrogen assisted crack initiation and propagation in a nickel-based superalloy, Acta Mater. 113 (2016) 272–283. doi:10.1016/j.actamat.2016.05.003.
[40] J. Rehrl, K. Mraczek, A. Pichler, E. Werner, Mechanical properties and fracture behavior of hydrogen charged AHSS/UHSS grades at high- and low strain rate tests, Mater. Sci. Eng. A. 590 (2014) 360–367. doi:10.1016/j.msea.2013.10.044.
[41] B. Bal, B. Okdem, F.C. Bayram, M. Aydin, A detailed investigation of the effect of hydrogen on the mechanical response and microstructure of Al 7075 alloy under medium strain rate impact loading, Int. J. Hydrogen Energy. 45 (2020) 25509–25522. doi:10.1016/j.ijhydene.2020.06.241.
[42] B. Bal, B. Çetin, F.C. Bayram, E. Billur, Effect of hydrogen on fracture locus of Fe–16Mn–0.6C–2.15Al TWIP steel, Int. J. Hydrogen Energy. (2020). doi:10.1016/j.ijhydene.2020.09.083.
[43] A. Laureys, T. Depover, R. Petrov, K. Verbeken, Characterization of hydrogen induced cracking in TRIP-assisted steels, in: Int. J. Hydrogen Energy, Elsevier Ltd, 2015: pp. 16901–16912. doi:10.1016/j.ijhydene.2015.06.017.
[44] B. Bal, I. Sahin, A. Uzun, D. Canadinc, A New Venue Toward Predicting the Role of Hydrogen Embrittlement on Metallic Materials, Metall. Mater. Trans. A Phys. Metall. Mater. Sci. 47 (2016) 5409–5422. doi:10.1007/s11661-016-3708-z.
[45] S.K. Dwivedi, M. Vishwakarma, Hydrogen embrittlement in different materials: A review, Int. J. Hydrogen Energy. 43 (2018) 21603–21616. doi:10.1016/j.ijhydene.2018.09.201.
[46] M.L. Martin, M. Dadfarnia, A. Nagao, S. Wang, P. Sofronis, Enumeration of the hydrogen-enhanced localized plasticity mechanism for hydrogen embrittlement in structural materials, Acta Mater. 165 (2019) 734–750. doi:10.1016/j.actamat.2018.12.014.

[47] I.M. Robertson, P. Sofronis, A. Nagao, M.L. Martin, S. Wang, D.W. Gross, K.E. Nygren, Hydrogen Embrittlement Understood, Metall. Mater. Trans. A Phys. Metall. Mater. Sci. 46 (2015) 2323–2341. doi:10.1007/s11661-015-2836-1.
[48] X. Li, X. Ma, J. Zhang, E. Akiyama, Y. Wang, X. Song, Review of Hydrogen Embrittlement in Metals: Hydrogen Diffusion, Hydrogen Characterization, Hydrogen Embrittlement Mechanism and Prevention, Acta Metall. Sin. (English Lett. 33 (2020) 759–773. doi:10.1007/s40195-020-01039-7.
[49] R.A. Oriani, A mechanistic theory of hydrogen embrittlement of steels, Berichte Der Bunsengesellschaft Für Phys. Chemie. 76 (1972) 848–857. doi:10.1002/BBPC.19720760864.
[50] M.B. Djukic, G.M. Bakic, V. Sijacki Zeravcic, A. Sedmak, B. Rajicic, The synergistic action and interplay of hydrogen embrittlement mechanisms in steels and iron: Localized plasticity and decohesion, Eng. Fract. Mech. 216 (2019) 106528. doi:10.1016/j.engfracmech.2019.106528.
[51] A. Nagao, M. Dadfarnia, B.P. Somerday, P. Sofronis, R.O. Ritchie, Hydrogen-enhanced-plasticity mediated decohesion for hydrogen-induced intergranular and "quasi-cleavage" fracture of lath martensitic steels, J. Mech. Phys. Solids. 112 (2018) 403–430. doi:10.1016/j.jmps.2017.12.016.
[52] P. Novak, R. Yuan, B.P. Somerday, P. Sofronis, R.O. Ritchie, A statistical, physical-based, micro-mechanical model of hydrogen-induced intergranular fracture in steel, J. Mech. Phys. Solids. 58 (2010) 206–226. doi:10.1016/J.JMPS.2009.10.005.
[53] I. Benedetti, V. Gulizzi, A. Milazzo, Grain-boundary modelling of hydrogen assisted intergranular stress corrosion cracking, Mech. Mater. 117 (2018) 137–151. doi:10.1016/j.mechmat.2017.11.001.
[54] R. Dutton, K. Nuttall, M.P. Puls, L.A. Simpson, MECHANISMS OF HYDROGEN INDUCED DELAYED CRACKING IN HYDRIDE FORMING MATERIALS., Met. Trans A. 8 A (1977) 1553–1562. doi:10.1007/BF02644858.
[55] C.D. Beachem, A new model for hydrogen-assisted cracking (hydrogen "embrittlement"), Metall. Trans. 3 (1972) 441–455. doi:10.1007/BF02642048.
[56] H.K. Birnbaum, P. Sofronis, Hydrogen-enhanced localized plasticity-a mechanism for hydrogen-related fracture, Mater. Sci. Eng. A. 176 (1994) 191–202. doi:10.1016/0921-5093(94)90975-X.
[57] P.J. Ferreira, I.M. Robertson, H.K. Birnbaum, Hydrogen effects on the interaction between dislocations, Acta Mater. 46 (1998) 1749–1757. doi:10.1016/S1359-6454(97)00349-2.
[58] I.M. Robertson, H.K. Birnbaum, An HVEM study of hydrogen effects on the deformation and fracture of nickel, Acta Metall. 34 (1986) 353–366. doi:10.1016/0001-6160(86)90071-4.
[59] J. Song, W.A. Curtin, Atomic mechanism and prediction of hydrogen embrittlement in iron, Nat. Mater. 12 (2013) 145–151. doi:10.1038/nmat3479.
[60] J. Song, W.A. Curtin, A nanoscale mechanism of hydrogen embrittlement in metals, Acta Mater. 59 (2011) 1557–1569. doi:10.1016/J.ACTAMAT.2010.11.019.
[61] S. Morita, K. Kitagawa, Y. Miyata, Hydration Structure of a Nafion Membrane in a Polymer Electrolyte Fuel Cell, in: 46th AIAA/ASME/SAE/ASEE Jt. Propuls. Conf. & Exhib., American Institute of Aeronautics and Astronautics, Reston, Virigina, 2010. doi:10.2514/6.2010-6922.
[62] R. Matsumoto, S. Taketomi, S. Matsumoto, N. Miyazaki, Atomistic simulations of hydrogen embrittlement, Int. J. Hydrogen Energy. 34 (2009) 9576–9584.

doi:10.1016/j.ijhydene.2009.09.052.
[63] X. Xing, G. Deng, H. Zhang, G. Cui, J. Liu, Z. Li, B. Wang, S. Li, C. Qi, Molecular Dynamics Studies of Hydrogen Effect on Intergranular Fracture in α-Iron, Materials (Basel). 13 (2020) 4949. doi:10.3390/ma13214949.
[64] S.P. Jung, Y. Kwon, C.S. Lee, B.J. Lee, Influence of hydrogen on the grain boundary crack propagation in bcc iron: A molecular dynamics simulation, Comput. Mater. Sci. 149 (2018) 424–434. doi:10.1016/j.commatsci.2018.03.053.
[65] X.Y. Zhou, X.S. Yang, J.H. Zhu, F. Xing, Atomistic simulation study of the grain-size effect on hydrogen embrittlement of nanograined Fe, Int. J. Hydrogen Energy. 45 (2020) 3294–3306. doi:10.1016/j.ijhydene.2019.11.131.
[66] Y. Zhu, Z. Li, M. Huang, Solute hydrogen effects on plastic deformation mechanisms of A-Fe with twist grain boundary, Int. J. Hydrogen Energy. 43 (2018) 10481–10495. doi:10.1016/j.ijhydene.2018.04.133.
[67] J. Song, W.A. Curtin, Mechanisms of hydrogen-enhanced localized plasticity: An atomistic study using α-Fe as a model system, Acta Mater. 68 (2014) 61–69. doi:10.1016/j.actamat.2014.01.008.
[68] Y. Zhu, Z. Li, M. Huang, H. Fan, Study on interactions of an edge dislocation with vacancy-H complex by atomistic modelling, Int. J. Plast. 92 (2017) 31–44. doi:10.1016/j.ijplas.2017.03.003.
[69] I.H. Katzarov, D.L. Pashov, A.T. Paxton, Hydrogen embrittlement I. Analysis of hydrogen-enhanced localized plasticity: Effect of hydrogen on the velocity of screw dislocations in α -Fe, Phys. Rev. Mater. 1 (2017) 1–11. doi:10.1103/PhysRevMaterials.1.033602.
[70] S. Plimpton, Fast parallel algorithms for short-range molecular dynamics, J. Comput. Phys. 117 (1995) 1–19. doi:10.1006/jcph.1995.1039.
[71] P. Franciosi, Glide mechanisms in b.c.c. crystals: An investigation of the case of α-iron through multislip and latent hardening tests, Acta Metall. 31 (1983) 1331–1342. doi:10.1016/0001-6160(83)90004-4.
[72] W.A. Spitzig, A.S. Keh, The effect of orientation and temperature on the plastic flow properties of iron single crystals, Acta Metall. 18 (1970) 611–622. doi:10.1016/0001-6160(70)90090-8.
[73] D. Scheiber, R. Pippan, P. Puschnig, L. Romaner, Ab initio calculations of grain boundaries in bcc metals, Model. Simul. Mater. Sci. Eng. 24 (2016) 35013. doi:10.1088/0965-0393/24/3/035013.
[74] M.S. Daw, M.I. Baskes, Semiempirical, quantum mechanical calculation of hydrogen embrittlement in metals, Phys. Rev. Lett. 50 (1983) 1285–1288. doi:10.1103/PhysRevLett.50.1285.
[75] A. Stukowski, Visualization and analysis of atomistic simulation data with OVITO–the Open Visualization Tool, Model. Simul. Mater. Sci. Eng. 18 (2010) 015012. doi:10.1088/0965-0393/18/1/015012.
[76] A. Stukowski, V. V Bulatov, A. Arsenlis, Automated identification and indexing of dislocations in crystal interfaces, Model. Simul. Mater. Sci. Eng. 20 (2012) 085007. doi:10.1088/0965-0393/20/8/085007.
[77] M. Zhou, A new look at the atomic level virial stress: On continuum-molecular system equivalence, Proc. R. Soc. A Math. Phys. Eng. Sci. 459 (2003) 2347–2392. doi:10.1098/rspa.2003.1127.
[78] M.F. Kapci, J.C. Schön, B. Bal, The role of hydrogen in the edge dislocation mobility and grain boundary-dislocation interaction in α -Fe , Int. J. Hydrogen Energy. (2021). doi:10.1016/j.ijhydene.2021.07.061.
[79] R. Peierls, The size of a dislocation, Proc. Phys. Soc. 52 (1940) 34–37.

doi:10.1088/0959-5309/52/1/305.
[80] J. Hirth, Theory of dislocations John Price Hirth [and] Jens Lothe., 1967.
[81] G. Monnet, D. Terentyev, Structure and mobility of the frac(1, 2) < 1 1 1 > {1 1 2} edge dislocation in BCC iron studied by molecular dynamics, Acta Mater. 57 (2009) 1416–1426. doi:10.1016/j.actamat.2008.11.030.
[82] S. Queyreau, J. Marian, M.R. Gilbert, B.D. Wirth, Edge dislocation mobilities in bcc Fe obtained by molecular dynamics, Phys. Rev. B - Condens. Matter Mater. Phys. 84 (2011) 1–7. doi:10.1103/PhysRevB.84.064106.
[83] G. Po, Y. Cui, D. Rivera, D. Cereceda, T.D. Swinburne, J. Marian, N. Ghoniem, A phenomenological dislocation mobility law for bcc metals, Acta Mater. 119 (2016) 123–135. doi:10.1016/j.actamat.2016.08.016.
[84] A.D. Brailsford, Anharmonicity contributions to dislocation drag, J. Appl. Phys. 43 (1972) 1380–1393. doi:10.1063/1.1661329.
[85] I.M. Robertson, M.L. Martin, J.A. Fenske, Influence of hydrogen on the behavior of dislocations, in: Gaseous Hydrog. Embrittlement Mater. Energy Technol. Mech. Model. Futur. Dev., Elsevier Inc., 2012: pp. 166–206. doi:10.1533/9780857095374.1.166.
[86] Chapter 4 Frictional forces in metals, in: Pergamon Mater. Ser., Elsevier Ltd, 2003: pp. 85–123. doi:10.1016/S1470-1804(03)80034-2.
[87] W. Xie, X. Liu, W. Chen, H. Zhang, Hydrogen hardening effect in heavily deformed single crystal α-Fe, Comput. Mater. Sci. 50 (2011) 3397–3402. doi:10.1016/j.commatsci.2011.06.036.
[88] Y. Zhao, M.Y. Seok, I.C. Choi, Y.H. Lee, S.J. Park, U. Ramamurty, J.Y. Suh, J. Il Jang, The role of hydrogen in hardening/softening steel: Influence of the charging process, Scr. Mater. 107 (2015) 46–49. doi:10.1016/j.scriptamat.2015.05.017.
[89] S. Taketomi, R. Matsumoto, S. Hagihara, Molecular statics simulation of the effect of hydrogen concentration on {112}<111> edge dislocation mobility in alpha iron, ISIJ Int. 57 (2017) 2058–2064. doi:10.2355/isijinternational.ISIJINT-2017-172.
[90] H. Matsui, H. Kimura, S. Moriya, The effect of hydrogen on the mechanical properties of high purity iron I. Softening and hardening of high purity iron by hydrogen charging during tensile deformation, Mater. Sci. Eng. 40 (1979) 207–216. doi:10.1016/0025-5416(79)90191-5.
[91] S. Taketomi, R. Matsumoto, N. Miyazaki, Atomistic study of the effect of hydrogen on dislocation emission from a mode II crack tip in alpha iron, Int. J. Mech. Sci. 52 (2010) 334–338. doi:10.1016/j.ijmecsci.2009.09.042.
[92] G. Zhou, F. Zhou, X. Zhao, W. Zhang, N. Chen, F. Wan, W. Chu, Molecular dynamics simulation of hydrogen enhancing dislocation emission, Sci. China, Ser. E Technol. Sci. 41 (1998) 176–181. doi:10.1007/bf02919680.
[93] J. Li, C. Lu, L. Pei, C. Zhang, R. Wang, Hydrogen-modified interaction between lattice dislocations and grain boundaries by atomistic modelling, Int. J. Hydrogen Energy. 45 (2020) 9174–9187. doi:10.1016/j.ijhydene.2020.01.103.
[94] I. Adlakha, K.N. Solanki, Critical assessment of hydrogen effects on the slip transmission across grain boundaries in α-Fe, Proc. R. Soc. A Math. Phys. Eng. Sci. 472 (2016). doi:10.1098/rspa.2015.0617.
[95] X.Y. Zhou, J.H. Zhu, H.H. Wu, X.S. Yang, S. Wang, X. Mao, Unveiling the role of hydrogen on the creep behaviors of nanograined α-Fe via molecular dynamics simulations, Int. J. Hydrogen Energy. 46 (2021) 9613–9629. doi:10.1016/j.ijhydene.2020.12.115.

[96] Y. He, Y. Li, C. Chen, H. Yu, Diffusion coefficient of hydrogen interstitial atom in A-Fe, Γ-Fe and ε-Fe crystals by first-principle calculations, Int. J. Hydrogen Energy. 42 (2017) 27438–27445. doi:10.1016/j.ijhydene.2017.08.212.
[97] K. Hirata, S. Iikubo, M. Koyama, K. Tsuzaki, H. Ohtani, First-Principles Study on Hydrogen Diffusivity in BCC, FCC, and HCP Iron, Metall. Mater. Trans. A Phys. Metall. Mater. Sci. 49 (2018) 5015–5022. doi:10.1007/s11661-018-4815-9.
[98] D.E. Jiang, E.A. Carter, Diffusion of interstitial hydrogen into and through bcc Fe from first principles, Phys. Rev. B - Condens. Matter Mater. Phys. 70 (2004). doi:10.1103/PhysRevB.70.064102.
[99] J. Sanchez, J. Fullea, C. Andrade, P.L. De Andres, Hydrogen in α -iron: Stress and diffusion, Phys. Rev. B - Condens. Matter Mater. Phys. 78 (2008) 014113. doi:10.1103/PhysRevB.78.014113.
[100] D. Di Stefano, M. Mrovec, C. Elsässer, First-principles investigation of quantum mechanical effects on the diffusion of hydrogen in iron and nickel, Phys. Rev. B - Condens. Matter Mater. Phys. 92 (2015) 224301. doi:10.1103/PhysRevB.92.224301.
[101] J. Greeley, M. Mavrikakis, A first-principles study of surface and subsurface H on and in Ni(1 1 1): Diffusional properties and coverage-dependent behavior, Surf. Sci. 540 (2003) 215–229. doi:10.1016/S0039-6028(03)00790-8.
[102] D. Connétable, J. Huez, É. Andrieu, C. Mijoule, First-principles study of diffusion and interactions of vacancies and hydrogen in hcp-titanium, J. Phys. Condens. Matter. 23 (2011) 405401. doi:10.1088/0953-8984/23/40/405401.
[103] Y. Lu, P. Zhang, First-principles study of temperature-dependent diffusion coefficients: Hydrogen, deuterium, and tritium in α-Ti, J. Appl. Phys. 113 (2013) 193502. doi:10.1063/1.4805362.
[104] N. Ehrlin, C. Bjerkén, M. Fisk, Cathodic hydrogen charging of Inconel 718, AIMS Mater. Sci. 3 (2016) 1350–1364. doi:10.3934/MATERSCI.2016.4.1350.
[105] E. V. Chatzidouros, V.J. Papazoglou, T.E. Tsiourva, D.I. Pantelis, Hydrogen effect on fracture toughness of pipeline steel welds, with in situ hydrogen charging, Int. J. Hydrogen Energy. 36 (2011) 12626–12643. doi:10.1016/J.IJHYDENE.2011.06.140.
[106] J.A. Ronevich, B.C. De Cooman, J.G. Speer, E. De Moor, D.K. Matlock, Hydrogen Effects in Prestrained Transformation Induced Plasticity Steel, Metall. Mater. Trans. A 2012 437. 43 (2012) 2293–2301. doi:10.1007/S11661-011-1075-3.
[107] O. Takakuwa, T. Ohmi, M. Nishikawa, A.T. Yokobori Jr., H. Soyama, Suppression of fatigue crack propagation with hydrogen embrittlement in stainless steel by cavitation peening, Strength, Fract. Complex. 7 (2011) 79–85. doi:10.3233/SFC-2011-0126.
[108] M. Hino, S. Mukai, T. Shimada, K. Okada, K. Horikawa, Inferences of Baking Time on Hydrogen Embrittlement for High Strength Steel Treated with Various Zinc Based Electroplating, Mater. Sci. Forum. 1016 (2021) 156–161. doi:10.4028/WWW.SCIENTIFIC.NET/MSF.1016.156.
[109] A. Oudriss, A. Fleurentin, G. Courlit, E. Conforto, C. Berziou, C. Rébéré, S. Cohendoz, J.M. Sobrino, J. Creus, X. Feaugas, Consequence of the diffusive hydrogen contents on tensile properties of martensitic steel during the desorption at room temperature, Mater. Sci. Eng. A. 598 (2014) 420–428. doi:10.1016/J.MSEA.2014.01.039.
[110] F. Galliano, E. Andrieu, C. Blanc, J.M. Cloue, D. Connetable, G. Odemer, Effect of trapping and temperature on the hydrogen embrittlement susceptibility of alloy

718, Mater. Sci. Eng. A. 611 (2014) 370–382. doi:10.1016/J.MSEA.2014.06.015.
[111] M.A. Mohtadi-Bonab, H. Ghesmati-Kucheki, Important Factors on the Failure of Pipeline Steels with Focus on Hydrogen Induced Cracks and Improvement of Their Resistance: Review Paper, Met. Mater. Int. 2019 255. 25 (2019) 1109–1134. doi:10.1007/S12540-019-00266-7.
[112] H.-J. Christ, M. Decker, S. Zeitler, Hydrogen diffusion coefficients in the titanium alloys IMI 834, Ti 10-2-3, Ti 21 S, and alloy C, Metall. Mater. Trans. A 2000 316. 31 (2000) 1507–1517. doi:10.1007/S11661-000-0161-8.
[113] J. Chene, F. Lecoester, A.M. Brass, D. Noel, SIMS analysis of deuterium diffusion in alloy 600: The correlation between fracture mode and deuterium concentration profile, Corros. Sci. 40 (1998) 49–60. doi:10.1016/S0010-938X(97)00110-8.
[114] M. Dadfarnia, A. Nagao, S. Wang, M.L. Martin, B.P. Somerday, P. Sofronis, Recent advances on hydrogen embrittlement of structural materials, Int. J. Fract. 2015 1961. 196 (2015) 223–243. doi:10.1007/S10704-015-0068-4.
[115] H. Shoda, H. Suzuki, K. Takai, Y. Hagihara, Hydrogen Desorption Behavior of Pure Iron and Inconel 625 during Elastic and Plastic Deformation, ISIJ Int. 50 (2010) 115–123. doi:10.2355/ISIJINTERNATIONAL.50.115.
[116] H.-J. Kim, H.-K. Park, C.-W. Lee, B.-G. Yoo, H.-Y. Jung, Baking Effect on Desorption of Diffusible Hydrogen and Hydrogen Embrittlement on Hot-Stamped Boron Martensitic Steel, Met. 2019, Vol. 9, Page 636. 9 (2019) 636. doi:10.3390/MET9060636.
[117] L. Zhang, Z. Li, J. Zheng, Y. Zhao, P. Xu, C. Zhou, C. Zhou, X. Chen, Dependence of hydrogen embrittlement on hydrogen in the surface layer in type 304 stainless steel, Int. J. Hydrogen Energy. 39 (2014) 20578–20584. doi:10.1016/J.IJHYDENE.2014.03.254.
[118] P. Nikolaidis, A. Poullikkas, A comparative overview of hydrogen production processes, Renew. Sustain. Energy Rev. 67 (2017) 597–611. doi:10.1016/j.rser.2016.09.044.
[119] A.M. Abdalla, S. Hossain, O.B. Nisfindy, A.T. Azad, M. Dawood, A.K. Azad, Hydrogen production, storage, transportation and key challenges with applications: A review, Energy Convers. Manag. 165 (2018) 602–627. doi:10.1016/j.enconman.2018.03.088.
[120] J.O. Abe, A.P.I. Popoola, E. Ajenifuja, O.M. Popoola, Hydrogen energy, economy and storage: Review and recommendation, Int. J. Hydrogen Energy. 44 (2019) 15072–15086. doi:10.1016/j.ijhydene.2019.04.068.
[121] A. Schneemann, J.L. White, S. Kang, S. Jeong, L.F. Wan, E.S. Cho, T.W. Heo, D. Prendergast, J.J. Urban, B.C. Wood, M.D. Allendorf, V. Stavila, Nanostructured Metal Hydrides for Hydrogen Storage, Chem. Rev. 118 (2018) 10775–10839. doi:10.1021/acs.chemrev.8b00313.
[122] W.I.F. David, Effective hydrogen storage: A strategic chemistry challenge, Faraday Discuss. 151 (2011) 399–414. doi:10.1039/c1fd00105a.

CURRICULUM VITAE

2013 – 2018 B.Sc., Mechanical Engineering, Abdullah Gül University, Kayseri, TURKEY

2018 – Present M.Sc., Advanced Materials and Nanotechnology, Abdullah Gül, Kayseri, TURKEY

2019 – Present Research Assistant, Mechanical Engineering, Abdullah Gül University, Kayseri, TURKEY

SELECTED PUBLICATIONS AND PRESENTATIONS

J1) M.F. Kapci, J.C. Schön, B. Bal, The role of hydrogen in the edge dislocation mobility and grain boundary-dislocation interaction in α -Fe , Int. J. Hydrogen Energy. (2021). doi:10.1016/j.ijhydene.2021.07.061.

J2) O. Dogan, M.F. Kapci, V. Esat, B. Bal, Experimental and Molecular Dynamics Simulation-Based Investigations on Hydrogen Embrittlement Behavior of Chromium Electroplated 4340 Steel, J. Eng. Mater. Technol. 143 (2021). doi:10.1115/1.4051400.

J3) F.C. Bayram, M.F. Kapçı, A. Yuruk, I.A. Isoglu, B. Bal, Investigations of strain rate, size, and crack length effects on the mechanical response of polycaprolactone electrospun membranes:, Https://Doi.Org/10.1177/09544089211024065. (2021). doi:10.1177/09544089211024065.

C1) M.F. Kapci, R. Unal, Design of bio-joint shaped knee exoskeleton assisting for walking and sit-to-stance, in: Biosyst. Biorobotics, Springer International Publishing, 2019: pp. 495–499. doi:10.1007/978-3-030-01887-0_96.

C2) J. Yao, P. Zhu, J. Ren, M.F. Kapçı, B. Bal, S. Kurko, Z. Wu, Z. Zhang, Numerical study of magnesium-based metal hydride reactor incorporating multi-phase heat exchanger for thermal energy storage system, in: Int. Conf. Appl. Energy, 2020.

C3) P. Zhu, L. Guo, J. Yao, J. Ren, M.F. Kapçı, B. Bal, Z. Wu, Z. Zhang, Parameter analysis of a biomass based SOFC-Engine polygeneration system for cooling, heating and power production, in: Int. Conf. Appl. Energy, 2020.